



Algorithm Theoretical Basis Document for Cloud Micro Physics of the NWC/PPS

NWC/CDOP3/PPS/SMHI/SCI/ATBD/CMIC, Issue 3, Rev. 1.0


01 September 2022

Applicable to SAFNWC/PPS version v2021

Applicable to the following PGEs:


Acronym	Product ID	Product name	Version number
CMIC	NWC-082	Cloud Microphysics	2.1

Prepared by Swedish Meteorological and Hydrological Institute (SMHI)

	Algorithm Theoretical Basis Document for Cloud Micro Physics of the NWC/PPS	Code: NWC/CDOP3/PPS/SMHI/SCI/ATBD/CMIC Issue: 3.1.0 Date: 01 September 2022 File: NWC-CDOP3-PPS-SMHI-SCI-ATBD-CMIC_v3_1_0 Page: 2/49
---	---	--

REPORT SIGNATURE TABLE


Function	Name	Signature	Date
Prepared by	Jan Fokke Meirink (KNMI, CMSAF) Ronald Scheirer (SMHI, NWCSAF) Updates by SMHI		01 September 2022
Reviewed by	SAFNWC Project Team EUMETSAT		For v2021: 28 September 2021 For EPS-SG: 27 March 2020
Authorised by	Nina Håkansson, SMHI <i>SAFNWC PPS Manager</i>		01 September 2022

	Algorithm Theoretical Basis Document for Cloud Micro Physics of the NWC/PPS	Code: NWC/CDOP3/PPS/SMHI/SCI/ATBD/CMIC Issue: 3.1.0 Date: 01 September 2022 File: NWC-CDOP3-PPS-SMHI-SCI-ATBD-CMIC_v3_1_0 Page: 3/49
---	---	--

DOCUMENT CHANGE RECORD

Version	Date	Pages	Changes
1.0d	22 January 2014	37	Replacing CDOP-document: SAF/NWC/CDOP/SMHI-PPS/SCI/ATBD/5 First version for SAFNWC/PPS v2014. Changes: <ul style="list-style-type: none"> - new document structure - inclusion of scientific updates (summarized in Section 1.6) - added a section describing output, including flags
1.0	15 September 2014	38	Response to Actions and RIDs from PCR2014. <ul style="list-style-type: none"> - Action 4: Provided rationale for using the DAK radiative transfer model in Section 4.2. - Act.7: Both operational and re-processed OSISAF ice maps can be used. - RID LSc-1; formal issues - RID LSc-2: Added a summary of requirements. - RID LSc-6: Replaced term ‘cloud type’ by ‘extended cloud phase’ to avoid confusion with the cloud type PGE throughout the document - RID LSc-9: Clarified the use of mid-latitude summer profiles in Section 4.2 and include ozone climatology as input dataset in Section 4.5.2. - RID LSc-12: Clarified in Section 5 that phase is retrieved during day and night - RID PW-37: Clarified correction of ice particle shape in Section 1.6. - RID PW-38: Explained pseudo-spherical correction in Section 4.2 - RID PW-39: Elaborated the NIR reflectance and emissivity in Section 4.3.1 - RID PW-40: Added introductory sentences in Section 4.3.2 - RID PW-41: Clarified cloudy-sky COT in Section 4.4
2.0d	23 December 2016	40	First version for SAFNWC/PPS v2018 Changes: <ul style="list-style-type: none"> - Introduced application to MODIS as a proxy for MERSI-2. - Can run on VIIRS data using a mix of I- and M-band channels. - Some additional minor corrections.
2.0	20 February 2017	39	Implemented RIDs from PCR-v2018: -Lutz-29: Corrected sub-section numbering in section 4.5.2.
2.1beta	9 May 2018	40	Document code changed from NWC/CDOP2/PPS/SMHI/SCI/ATBD/5 to NWC/CDOP3/PPS/SMHI/SCI/ATBD/5. Changes for v2018: -Alternative input: CMa-prob. Some alternatives for CTTH-input as well.
2.1d	17 October 2018	39	Changes for SAFNWC/PPS-v2018 ORR: -Updated scientific references. -Added TBD01, about MERSI-2 usage.
2.1	13 December 2018	40	Updates after v2018 ORR: OBJ2_UM_SCI_Heinemann_039: Removed most PGE-<number> notations in this document. OBJ2_UM_SCI_Heinemann_041: editorial Other changes: Describe configuration SM_CMAPROB_CLOUD_THRESHOLD.
2.2d	20 February 2020	42	Preparation for PPS v2018.x (x>2) <ul style="list-style-type: none"> -Can process for MERSI2 data. (Closing TBD01) -Including development from CMSAF feed-back loop. - Inclusion of CDNC and CGT as by-products - Revised and extended uncertainty estimates - Several smaller algorithm updates

1.0d	21 February 2020	46	<p>First version for EPS-SG. Replacing document: NWC/CDOP3/PPS/SMHI/SCI/ATBD/PPS.</p> <ul style="list-style-type: none"> -Added usage of METImage data. -Start using a few channels, which are not AVHRR-heritage, for METImage and VIIRS. -Changed product name from Cloud Physical Properties (CPP) to Cloud Microphysics (CMIC). -Changed dataset name from REFF to CRE. (Cloud Particle Effective Radius)
NWC/CDO P3/EPSSG/SMHI/SCI/ATBD/CMIC 1.0	15 April 2020	49	<p>Changes related to PDCR RIDs:</p> <ul style="list-style-type: none"> -OBJ6_ATBD_Schluessel_001, 002: Clarifications about the calculations and assumptions. -OBJ6_ATBD_Schluessel_003: Giving a more detailed description of the usage of channel 2.25μm. -OBJ6_ATBD_Schluessel_004: Use different cloud phase algorithm for METImage, than was used for AVHRR. In order to make better use of the spectral information available.
NWC/CDO P3/PPS/SMHI/SCI/ATBD/CMIC 3.0d	22 March 2021	49	<p>Changes related both to v2021 and vEPSSG:</p> <ul style="list-style-type: none"> - Added AVHRR/1 usage. -The radiative transfer look-up tables have been modified based on different choices for ice particle habits and size distribution and water droplet size distribution width. -Changed effective variance used for cloud droplets. -For input data snow depth and ice concentration, now use a gradual increase. -Replaced the input dataset surface albedo, from one MODIS version to another. <p>Changes specially for vEPSSG:</p> <ul style="list-style-type: none"> -For cmic_phase_extended added the class overshooting. -Corrected the description of the METImage resolution. <p>Changes specially for v2021:</p> <ul style="list-style-type: none"> - Describe that v2021 does not work for METImage (TBD02) - Describe that v2021 for VIIRS only uses the AVHRR-heritage channels. <p>Document improvement:</p> <ul style="list-style-type: none"> - Some clarifications in the text. (some of them as a response to a CMSAF-review) -Corrected a typo in table 8. -Corrected a typo in equation 21. -Updated scientific references to match other changes.
NWC/CDO P3/PPS/SMHI/SCI/ATBD/CMIC 3.0e	26 April 2021	49	<p>Changes after PPS v2021 RR:</p> <ul style="list-style-type: none"> - Make clearer the status of processing for: MERSI-2 and METImage. - RID-1: Added more explanations in section 4.1 - RID-2, 16, 18: editorial - RID-6: Added more details about the plans for METImage. - RID-15: Described that section 4.2.1 "Infrared radiative transfer for cloud phase" is not relevant for PPS v2021, and will be reconsidered. - RID-17: clarification on METImage resolution <p>Please note that RID-4 has not been implemented yet.</p>
NWC/CDO P3/PPS/SMHI/SCI/ATBD/CMIC 3.0e	1 September 2021	48	<p>Changes before PPS v2021 DRR:</p> <ul style="list-style-type: none"> - Addressed Action-004 by discussion of the impact of RTM errors on CMIC errors, in particular for cloud phase -Updated section 4.2 to be in line with RR discussion result on "Risk of violating timeliness requirements" (agreed not to change of phase algorithm for Metimage, specifically not introducing online RT calculations) - RID-15 Updated section 4.3.1.2: discuss which channels have potential to better exploit the METImage capabilities (Recommendation-02) from day-2 for phase, and aligned phase algorithm description with implementation agreed for Versions 2021/EPS-SG day one. Supersedes previous changes introduced for RID 15. -Updated TBD02 with current plans.

	<p>Algorithm Theoretical Basis Document for Cloud Micro Physics of the NWC/PPS</p>	<p>Code:NWC/CDOP3/PPS/SMHI/SCI/ATBD/CMIC Issue: 3.1.0 Date: 01 September 2022 File: NWC-CDOP3-PPS-SMHI-SCI-ATBD-CMIC_v3_1_0 Page: 5/49</p>
---	--	---

NWC/CDO P3/PPS/SM HI/SCI/AT BD/CMIC 3.0	12 October 2021	48	Changes after PPS v2021 DRR: -RID 42: Replace ‘CPP’ with ‘CMIC’, in the text, where relevant.
NWC/CDO P4/EPSSG/ SMHI/SCI/ ATBD/CMIC C 1.1.0	9 March 2022	49	Changes for vEPSSG SIRR: -CMIC runs for METImage, and channel 2.2µm can now be used. Closing TBD02. -Adding TBD03 for future development regarding METImage.
NWC/CDO P3/PPS/SM HI/SCI/AT BD/CMIC 3.1.0	01 September 2022	49	The version for v2021-patch2 is identical as for vEPSSG SIRR, except for document code and version. References are updated. In ‘Scientific Updates’ is clarified what is applicable for PPS v2021.2.



	Algorithm Theoretical Basis Document for Cloud Micro Physics of the NWC/PPS	Code: NWC/CDOP3/PPS/SMHI/SCI/ATBD/CMIC Issue: 3.1.0 Date: 01 September 2022 File: NWC-CDOP3-PPS-SMHI-SCI-ATBD-CMIC_v3_1_0 Page: 6/49
---	---	--

Table of Contents

1. INTRODUCTION	9
1.1. PURPOSE.....	9
1.2. SCOPE.....	9
1.3. DEFINITIONS AND ACRONYMS	9
1.4. REFERENCES.....	12
1.4.1. Applicable documents.....	12
1.4.2. Reference documents.....	12
1.4.3. Scientific References.....	13
1.5. DOCUMENT OVERVIEW	17
1.6. SCIENTIFIC UPDATES SINCE PPS VERSION 2018.....	17
2. INTRODUCTION TO THE SAFNWC/PPS CLOUD MICROPHYSICS PRODUCT.....	18
2.1. REQUIREMENTS	18
3. ALGORITHM OVERVIEW	20
4. ALGORITHM DESCRIPTION.....	20
4.1. THEORETICAL DESCRIPTION	20
4.2. RADIATIVE TRANSFER	22
4.3. RETRIEVAL SCHEME	27
4.3.1. Cloud phase.....	28
4.3.1.1 AVHRR.....	28
4.3.1.2 METimage	30
4.3.2. Cloud optical properties.....	30
4.4. ERROR BUDGET ESTIMATES	31
4.5. PRACTICAL APPLICATION	36
4.5.1. Satellite instruments	37
4.5.2. Input data	39
4.5.2.1 Radiances	39
4.5.2.2 Solar and satellite angles	39
4.5.2.3 Cloud mask	39
4.5.2.4 Cloud top height and temperature	39
4.5.2.5 Surface albedo	40
4.5.2.6 Surface emissivity	40
4.5.2.7 Numerical Weather Prediction (NWP) model fields	40
4.5.2.8 Sea ice concentration.....	41
4.5.2.9 Ozone	41
4.5.3. Description of Output.....	41
5. ASSUMPTIONS AND LIMITATIONS	43
ANNEX A. LIST OF TBC, TBD, OPEN POINTS AND COMMENTS.....	46
ANNEX B. THRESHOLDS USED IN THE CLOUD PHASE ALGORITHM.....	47

List of Tables and Figures

TABLE 1 LIST OF ACRONYMS AND ABBREVIATIONS	11
TABLE 2: LIST OF APPLICABLE DOCUMENTS	12
TABLE 3: LIST OF REFERENCED DOCUMENTS	13
TABLE 4: OVERVIEW OF SAF PRODUCTS COVERED IN THIS ATBD.	18
TABLE 5 ACCURACY REQUIREMENTS FOR CMIC CLOUD PHASE	19
TABLE 6 ACCURACY REQUIREMENTS FOR CMIC LIQUID WATER PATH	19
TABLE 7 PROPERTIES OF THE CLOUDY ATMOSPHERE THAT ARE USED FOR THE RADIATIVE TRANSFER CALCULATIONS TO GENERATE THE LUTs.	25
TABLE 8 TYPICAL MAGNITUDE OF ATMOSPHERIC CORRECTION, EXPRESSED AS 1 MINUS THE TWO-WAY TRANSMISSIVITY, IN %. THE NUMBERS HAVE BEEN CALCULATED FOR A REFERENCE ATMOSPHERE ($H_c = 2$ KM, $AMF = 2$, $TCO = 332$ DU, AND $WVP = 30$ KG M ⁻²), BASED ON THE NOAA-15 AVHRR SPECTRAL RESPONSE, AND FOR INDIVIDUAL ABSORBING GASES AS WELL AS FOR ALL GASES TOGETHER.	26
TABLE 9: ERROR SOURCES TAKEN INTO ACCOUNT FOR CMIC RETRIEVAL UNCERTAINTY ESTIMATES.	33
TABLE 10: RELATIVE UNCERTAINTIES (IN %) IN COT AND CRE RETRIEVALS AS A TOTAL AND SEPARATED BY ERROR SOURCE. THE NUMBERS REFLECT THE MEDIAN UNCERTAINTIES FROM A FULL DISK WORTH OF SEVIRI RETRIEVALS (7 MARCH 2017, 14:00 UTC). PIXELS FOR WHICH THE OBSERVATIONS WERE OUTSIDE THE LOOK-UP TABLE OR THE VISIBLE SURFACE ALBEDO WAS LARGER THAN 0.6 WERE EXCLUDED. RESULTS ARE SHOWN SEPARATELY FOR THE 0.6–1.6 μ M AND THE 0.6–3.8 μ M RETRIEVALS AS WELL AS FOR LIQUID AND ICE CLOUDS. ROWS WITH A GREY BACKGROUND CONTAIN THE MAIN ERROR SOURCES, SOME OF WHICH HAVE BEEN FURTHER SEPARATED AS SHOWN IN THE ROWS WITH A WHITE BACKGROUND. THE TOTAL UNCERTAINTY AND THE INDIVIDUAL ERROR SOURCE CONTRIBUTING MOST TO THE TOTAL UNCERTAINTY ARE INDICATED IN BOLD FACE.	34
TABLE 11: AVHRR CHANNELS USED BY CMIC	37
TABLE 12: VIIRS CHANNELS USED BY CMIC.	37
TABLE 13: VIIRS CHANNELS USED BY CMIC, FOR RUNNING IN HIGH RESOLUTION.	38
TABLE 14: MODIS CHANNELS USED BY CMIC.	38
TABLE 15: MERIS-2 CHANNELS USED BY CMIC.	38
TABLE 16: METIMAGE CHANNELS USED BY CMIC.	38
TABLE 17 CMIC CONDITIONS AND PROCESSING FLAGS	42
FIGURE 1 SIMULATED TOP-OF-ATMOSPHERE (TOA) REFLECTANCE SPECTRA FOR A STRATOCUMULUS (WATER) CLOUD AND A CIRRUS (ICE) CLOUD, AND THE IMAGINARY PART OF THE INDEX OF REFRACTION OF WATER AND ICE. THE SIMULATIONS WERE MADE WITH THE MODERATE RESOLUTION ATMOSPHERIC TRANSMITTANCE AND RADIANCE CODE (MODTRAN) AT $\theta_0 = 45^\circ$, $\theta = 0^\circ$ AND $\Phi = 0^\circ$. THE REFLECTANCES ARE PLOTTED AS BLACK LINES, WHILE THE REFRACTIVE INDICES ARE PLOTTED AS GRAY LINES.	22
FIGURE 2: COMPARISON BETWEEN SCATTERING PHASE FUNCTIONS OF THE SEVERELY ROUGHENED AGGREGATE SOLID COLUMN HABIT, IMPERFECT (ROUGHENED) HEXAGONS, PERFECT (SMOOTH) HEXAGONS, AND WATER DROPLETS. THE WAVELENGTH IS 0.64 μ M AND THE EFFECTIVE RADII ARE 12 μ M FOR THE WATER DROPLETS AND 10 μ M FOR THE ICE CRYSTALS.	24
FIGURE 3: ASYMMETRY PARAMETER (LEFT) AND SINGLE SCATTERING ALBEDO (RIGHT) AS A FUNCTION OF CLOUD PARTICLE EFFECTIVE RADIUS FOR THE AGGREGATE SOLID COLUMN AND IMPERFECT HEXAGON HABITS AS WELL AS LIQUID CLOUD DROPLETS. RESULTS ARE SHOWN FOR THREE WAVELENGTHS: 0.6, 1.6 AND 3.8 μ M.	24
FIGURE 4 DAK CALCULATIONS OF TOA REFLECTANCE AT 0.6 μ M VERSUS 1.6 μ M (TOP LEFT), 2.2 μ M (TOP RIGHT) AND 3.8 μ M (BOTTOM) FOR CLOUDS CONSISTING OF SPHERICAL WATER DROPLETS (RED CURVES) AND ROUGHENED, AGGREGATE SOLID ICE COLUMNS (BLUE CURVES). THE REFLECTANCES HAVE BEEN CALCULATED OVER A BLACK SURFACE (ALBEDO = 0). SOLAR AND SATELLITE ANGLES ARE INDICATED IN THE PLOTS. THE VERTICALLY ORIENTED LINES REPRESENT LINES OF EQUAL CLOUD OPTICAL THICKNESS, WHILE THE HORIZONTALLY ORIENTED LINES REPRESENT LINES OF EQUAL PARTICLE SIZE. VALUES OF OPTICAL THICKNESS AND CLOUD PARTICLE EFFECTIVE RADIUS ARE INDICATED IN THE PLOT. NOTE THE DIFFERENT SCALING OF THE VERTICAL AXIS IN BOTH PANELS.	25
FIGURE 5: DEPENDENCE OF COT AND CRE UNCERTAINTIES ON COT AND CRE OF BOTH LIQUID AND ICE CLOUDS FOR THE 0.6–1.6 MICRON RETRIEVAL. UNCERTAINTIES DUE TO DIFFERENT ERROR SOURCES ARE SHOWN SEPARATELY. COT AND CRE HISTOGRAMS ARE INDICATED BY THE GREY LINES.	35
FIGURE 6: AS FIGURE 5, BUT FOR THE 0.6–3.8 MICRON RETRIEVAL.	36
FIGURE 7: COT AND CRE UNCERTAINTIES AS A FUNCTION OF SOLAR ZENITH ANGLE (LEFT) AND VIS SURFACE ALBEDO (RIGHT). COT AND CRE HISTOGRAMS ARE INDICATED BY THE GREY LINES.	36

	Algorithm Theoretical Basis Document for Cloud Micro Physics of the NWC/PPS	Code: NWC/CDOP3/PPS/SMHI/SCI/ATBD/CMIC Issue: 3.1.0 Date: 01 September 2022 File: NWC-CDOP3-PPS-SMHI-SCI-ATBD-CMIC_v3_1_0 Page: 9/49
---	---	--

1. INTRODUCTION

The EUMETSAT “Satellite Application Facilities” (SAF) are dedicated centres of excellence for processing satellite data, and form an integral part of the distributed EUMETSAT Application Ground Segment (<http://www.eumetsat.int>). This documentation is provided by the SAF on Support to Nowcasting and Very Short Range Forecasting, SAFNWC. The main objective of SAFNWC is to provide, further develop and maintain software packages to be used for Nowcasting applications of operational meteorological satellite data by National Meteorological Services. More information can be found at the SAFNWC webpage, <http://nwc-saf.eumetsat.int>. This document is applicable to the SAFNWC processing package for polar orbiting meteorological satellites, SAFNWC/PPS, developed and maintained by SMHI (<http://nwcsaf.smhi.se>).

1.1. PURPOSE

This document is the Algorithm theoretical Basis Document for the Cloud Microphysics (CMIC) of the SAFNWC/PPS software package.

This document contains a description of the algorithm, including scientific aspects and practical considerations.

1.2. SCOPE

This document describes the algorithms implemented in the CMIC version 2.1 of the SAFNWC/PPS software package delivery, with product ID: NWC-082. The same algorithm will be applied in the CMIC version 3.0 of the EPS-SG SAFNWC/PPS software package delivery, with product ID: NWC-151. The official products of SAFNWC/PPS CMIC are: LWP and CPH. Additional products are: IWP, COT, CRE, CPH_extended, CDNC and CGT (the latter two only for liquid clouds).

It is also worth to notice that the software is developed by, and used in, CM-SAF. CM-SAF used the software (v1.0) for the generation of CLARA-A2 (CLoud Albedo and Radiation dataset using AVHRR, edition 2). Version 2.0 will be used for the production of the CLARA-A3 products. In CM-SAF the following product names and product IDs are used for the CLARA-A2 products CPH (CM-11042), LWP (CM-11052) and IWP (CM-11062). COT and CRE (REFF) are provided as by-products of LWP and IWP, while CDNC and CGT are provided as by-products of LWP. The algorithm used in version 2.1 is identical as the one used in CLARA-A3, but with some technical changes -matching different versions of PPS.

Please note that the output product is called Cloud Microphysics (CMIC), while the software producing it is called Cloud Physical Properties (CPP).

1.3. DEFINITIONS AND ACRONYMS

<i>EUMETSAT Satellite Application Facility to NoWcasting & Very Short Range Forecasting</i>	Algorithm Theoretical Basis Document for Cloud Micro Physics of the NWC/PPS	Code: NWC/CDOP3/PPS/SMHI/SCI/ATBD/CMIC Issue: 3.1.0 Date: 01 September 2022 File: NWC-CDOP3-PPS-SMHI-SCI-ATBD-CMIC_v3_1_0 Page: 10/49
---	---	---

Acronym	Explanation	Acronym	Explanation
ACPG	AVHRR/AMSU Cloud Product Generation software (A major part of the SAFNWC/PPS s.w., including the PGEs.)	IWP	Ice Water Path
AEMET	Agencia Estatal de Meteorología (Spain)	JPSS	Joint Polar Satellite System (US)
AVHRR	Advanced Very High Resolution Radiometer	KNMI	Koninklijk Nederlands Meteorologisch Instituut
CDNC	Cloud Droplet Number Concentration	LES	Large Eddy Simulation
CDOP	Continuous Development and Operational Phase	LUT	look-up-table
CDOP-3	Third Continuous Development and Operational Phase	LWP	Liquid Water Path
CGT	Cloud Geometrical Thickness	MERSI	Medium Resolution Spectral Imager
CM-SAF	Climate Monitoring SAF	METImage	Meteorological Imager
CMA	Cloud Mask (also PGE01)	MODIS	Moderate Resolution Imaging Spectroradiometer
CMa-prob	Cloud Probability (also PGE01c)	MODTRAN	MODerate spectral resolution atmospheric TRANsmittance and radiance code
CMIC	Cloud Micro-physics The CPP s.w. produces the CMIC product.	MSG	Meteosat Second Generation
COT (or τ)	Cloud Optical Thickness	NOAA	National Oceanic and Atmospheric Administration
CPH	Cloud thermodynamic Phase	NPP	NPOESS Preparatory Project (relates also to JPSS)
CPP	Cloud Physical Properties The CPP s.w. produces the CMIC product.	PC	Precipitating Cloud (also PGE04) (previously a PPS product)
CRE (or r_e)	Cloud particle Effective Radius. Alternative abbreviation for REFF.	PGE	Process Generating Element
CT	Cloud Type (also PGE02)	PPS	Polar Platform System
CTTH	Cloud Top Temperature, Height and Pressure (also PGE03)	REFF (or r_e)	Cloud Particle Effective radius Alternative abbreviation for CRE.
CWP	Cloud Water Path	RTM	Radiative Transfer Model
DAK	Doubling Adding KNMI	RTTOV	Radiative Transfer for TOVS
DISORT	Discrete Ordinate	SAF	Satellite Application Facility
EPS	EUMETSAT Polar System	SAFNWC	Satellite Application Facility for support to NoWcasting
EPS-SG	EPS Second Generation	SEVIRI	Spinning Enhanced Visible Infra-Red Imager
EUMETSAT	European Organisation for the Exploitation of Meteorological Satellites	SHDOM	Spherical Harmonic Discrete Ordinate Method
		SMHI	Swedish Meteorological and Hydrological Institute
		SW	SoftWare

<i>EUMETSAT Satellite Application Facility to NoWCasting & Very Short Range Forecasting</i>	Algorithm Theoretical Basis Document for Cloud Micro Physics of the NWC/PPS	Code: NWC/CDOP3/PPS/SMHI/SCI/ATBD/CMIC Issue: 3.1.0 Date: 01 September 2022 File: NWC-CDOP3-PPS-SMHI-SCI-ATBD-CMIC_v3_1_0 Page: 11/49
---	---	---

Acronym	Explanation	Acronym	Explanation
TBC	To Be Confirmed	TOA	Top Of Atmosphere
TBD	To Be Defined	VIIRS	Visible Infrared Imaging Radiometer Suite

Table 1 List of acronyms and abbreviations

<i>EUMETSAT Satellite Application Facility to NoWCasting & Very Short Range Forecasting</i>	Algorithm Theoretical Basis Document for Cloud Micro Physics of the NWC/PPS	Code: NWC/CDOP3/PPS/SMHI/SCI/ATBD/CMIC Issue: 3.1.0 Date: 01 September 2022 File: NWC-CDOP3-PPS-SMHI-SCI-ATBD-CMIC_v3_1_0 Page: 12/49
---	---	---

See [RD.1.] for a complete list of acronyms for the SAFNWC project.

1.4. REFERENCES

1.4.1. Applicable documents

The following documents, of the exact issue shown, form part of this document to the extent specified herein. Applicable documents are those referenced in the Contract or approved by the Approval Authority. They are referenced in this document in the form [AD.X]

For dated references, subsequent amendments to, or revisions of, any of these publications do not apply. For undated references, the current edition of the document referred applies.

Current documentation can be found at SAFNWC Helpdesk web: <http://nwc-saf.eumetsat.int>

Ref	Title	Code	Vers	Date
[AD.1.]	NWC SAF Product Requirements Document	NWC/CDOP3/SAF/AEMET/MGT/PRD	1.4	02/06/21
[AD.2.]	NWCSAF Project Plan	NWC/CDOP3/SAF/AEMET/MGT/PP	1.5	15/04/21
[AD.3.]	System and Components Requirements Document for the SAFNWC/PPS	NWC/CDOP3/PPS/SMHI/SW/SCRD	2.3	12/10/21

Table 2: List of Applicable Documents

1.4.2. Reference documents

The reference documents contain useful information related to the subject of the project. These reference documents complement the applicable ones, and can be looked up to enhance the information included in this document if it is desired. They are referenced in this document in the form [RD.X]

For dated references, subsequent amendments to, or revisions of, any of these publications do not apply. For undated references, the current edition of the document referred applies

Current documentation can be found at SAFNWC Helpdesk web: <http://nwc-saf.eumetsat.int>

<i>EUMETSAT Satellite Application Facility to NoWcasting & Very Short Range Forecasting</i>	Algorithm Theoretical Basis Document for Cloud Micro Physics of the NWC/PPS	Code: NWC/CDOP3/PPS/SMHI/SCI/ATBD/CMIC Issue: 3.1.0 Date: 01 September 2022 File: NWC-CDOP3-PPS-SMHI-SCI-ATBD-CMIC_v3_1_0 Page: 13/49
---	---	---

Ref	Title	Code	Vers	Date
[RD.1.]	The Nowcasting SAF Glossary	NWC/CDOP3/SAF/AEMET/MGT/GLO	1.0	20/10/20
[RD.2]	Validation Report AVHRR GAC cloud products, Edition 2	SAF/CM/DWD/VAL/GAC/CLD	2.3	18/11/16
[RD.3]	User Manual for the Cloud Product Processors of the SAFNWC/PPS: Science Part	NWC/CDOP3/PPS/SMHI/SCI/UM/Cloud	3.1.0	01/09/22
[RD.4]	Scientific and Validation report for the Cloud Product Processors of the NWC/PPS	NWC/CDOP3/PPS/SMHI/SCI/VR/Cloud	3.0	12/10/21
[RD.5]	Algorithm Theoretical Basis Document for the Cloud Mask of the NWC/PPS	NWC/CDOP3/PPS/SMHI/SCI/ATBD/Clo udMask	3.1.0	01/09/22
[RD.6]	Algorithm Theoretical Basis Document for the Cloud Top Temperature, Pressure and Height of the NWC/PPS	NWC/CDOP3/PPS/SMHI/SCI/ATBD/CT TH	3.1.0	01/09/22

Table 3: List of Referenced Documents

1.4.3. Scientific References

Ackerman, S.A., W.L. Smith, R.E. Revercomb, and J.D. Spinhirne, 1990: The 27–28 October 1986 FIRE IFO Cirrus Case Study: Spectral Properties of Cirrus Clouds in the 8–12 μm Window, *Mon. Wea. Rev.*, **118**, 2377–2388.

Anderson, G. P., S. A. Clough, F. X. Kneizys, J. H. Chetwynd, and E. P. Shettle, 1986: AFGL Atmospheric Constituent Profiles (0–120km). Tech. Rep. AFGL-TR-86-0110, 43 pp.

Baum, B. A., 2014: Ice cloud bulk scattering models, https://www.ssec.wisc.edu/ice_models/.

Baum, B. A., P. Yang, A. J. Heymsfield, C. G. Schmitt, Y. Xie, A. Bansemer, Y.-X. Hu, and Z. Zhang, 2011: Improvements in shortwave bulk scattering and absorption models for the remote sensing of ice clouds, *J. Appl. Meteorol. Clim.*, **50**, 1037–1056, doi:10.1175/2010JAMC2608.1.

Benas, N., Meirink, J. F., Stengel, M., and Stammes, P.: Sensitivity of liquid cloud optical thickness and effective radius retrievals to cloud bow and glory conditions using two SEVIRI imagers, *Atmospheric Measurement Techniques*, **12**, 2863–2879, doi:10.5194/amt-12-2863-2019, 2019.

Bennartz, R. and Rausch, J., 2017: Global and regional estimates of warm cloud droplet number concentration based on 13 years of AQUA-MODIS observations, *Atmos. Chem. Phys.*, **17**, 9815–9836, doi:10.5194/acp-17-9815-2017.

Berk, A., G. P. Anderson, P. K. Acharya, J. H. Chetwynd, L.S. Bernstein, E. P. Shettle, M. W. Matthew, and S. M. Adler-Golden, 2000: MODTRAN4 Version 2 Users Manual. Technical report, Air Force Materiel Command, Air Force Research Laboratory, Space Vehicles Directorate, Hanscom AFB, MA 01731, USA.

Borg, L. A. and Bennartz, R., 2007: Vertical structure of stratiform marine boundary layer clouds and its impact on cloud albedo. *Geophysical Research Letters*, **34**, doi: 10.1029/2006GL028713

Chandrasekhar S., 1960: *Radiative Transfer*, New York, Dover, 393 pp. Coakley, J. A., M. A. Friedman, and W. R. Tahnk, 2005: Retrieval of cloud properties for partly cloudy imager pixels, *J. Atmos. Ocean. Technol.*, **22**, 3–17.

De Haan, J. F., P. Bosma, and J. W. Hovenier, 1987: The adding method for multiple scattering calculations of polarized light, *Astron. Astrophys.*, **183**, 371–391.

Evans, K. F., 1998: The Spherical Harmonics Discrete Ordinate, Method for Three-Dimensional Atmospheric Radiative Transfer. *J. Atmos. Sci.*, **55**, 429–446.

Grosvenor, D.P., O. Soudervall, P. Zuidema, A.S. Ackerman, M.D. Alexandrov, R. Bennartz, R. Boers, B. Cairns, J.C. Chiu, M. Christensen, H. Deneke, M. Diamond, G. Feingold, A. Fridlind, A. Hünerbein, C. Knist, P. Kollias, A. Marshak, D. McCoy, D. Merk, D. Painemal, J. Rausch, D.

<i>EUMETSAT Satellite Application Facility to NoWCASTing & Very Short Range Forecasting</i>	Algorithm Theoretical Basis Document for Cloud Micro Physics of the NWC/PPS	Code: NWC/CDOP3/PPS/SMHI/SCI/ATBD/CMIC Issue: 3.1.0 Date: 01 September 2022 File: NWC-CDOP3-PPS-SMHI-SCI-ATBD-CMIC_v3_1_0 Page: 14/49
---	---	---

Rosenfeld, H. Russchenberg, P. Seifert, K. Sinclair, P. Stier, B. van Diedenhoven, M. Wendisch, F. Werner, R. Wood, Z. Zhang, and J. Quaas, 2018: Remote sensing of cloud droplet number concentration: Review of current and perspectives for new approaches. *Rev. Geophys.*, **56**, no. 2, 409–453, doi:10.1029/2017RG000593.

Håkansson, N., Adok, C., Thoss, A., Scheirer, R., and Hörnquist, S.: Neural network cloud top pressure and height for MODIS, *Atmos. Meas. Tech.*, **11**, 3177–3196, <https://doi.org/10.5194/amt-11-3177-2018>, 2018.

Haywood, J.M., S.R. Osborne, S.J. Abel, 2004: The effect of overlying absorbing aerosol layers on remote sensing retrievals of cloud effective radius and cloud optical depth, *Quart. J. Roy. Meteorol. Soc.*, **130**, 779–800, doi: 10.1256/qj.03.100.

Heidinger, A.K., W.C. Straka III, C.C. Molling, J.T. Sullivan, and X. Wu, 2010: Deriving an inter-sensor consistent calibration for the AVHRR solar reflectance data record, *Int. J. Remote Sensing*, **31**, 6493–6517, doi:10.1080/01431161.2010.496472.

Hess, H, R. B. A. Koelemeijer, and P. Stammes, 1998: Scattering matrices of imperfect hexagonal crystals. *J. Quant. Spectrosc. Radiat. Transfer*, **60**, 301–308.

Jin, Z., Y. Qiao, Y. Wang, Y. Fang, and W. Yi, 2011: A new parameterization of spectral and broadband ocean surface albedo, *Opt. Express*, **19**, 26429–26443, doi:10.1364/OE.19.026429.

Jolivet, D., and A. J. Feijt, 2003: Cloud thermodynamic phase and particle size estimation using the 0.67 and 1.6 micron channels from meteorological satellites. *Atm. Chem. Phys. Discuss.*, **3**, 4461–4488.

Karlsson, K.-G., Anttila, K., Trentmann, J., Stengel, M., Meirink, J. F., Devasthale, A., Hanschmann, T., Kothe, S., Jaaskelainen, E., Sedlar, J., Benas, N., van Zadelhoff, G.-J., Schlundt, C., Stein, D., Finkensieper, S., Hakansson, N., and Hollmann, R., 2017: CLARA-A2: the second edition of the CM SAF cloud and radiation data record from 34 years of global AVHRR data, *Atmospheric Chemistry and Physics*, **17**, 5809–5828, doi:10.5194/acp-17-5809-2017.

Macke, A., D. Mitchell, and L. von Bremen, 1999: Monte Carlo radiative transfer calculations for inhomogeneous mixed phase clouds. *Phys. Chem. Earth*, **24-3**, 237–241.

Marshak, A., S. Platnick, T. Várnai, G. Wen, and R. F. Cahalan, 2006: Impact of three-dimensional radiative effects on satellite retrievals of cloud droplet sizes, *J. Geophys. Res.*, **111**, 9207–9218.

McFarquhar, G.M. and A.J. Heymsfield, 1998: The definition and significance of an effective radius for ice clouds, *J. Atmos. Sci.*, **55**, 2039–2052.

Meirink, J.F., R.A. Roebeling and P. Stammes, 2009: Atmospheric correction for the KNMI Cloud Physical Properties retrieval algorithm, KNMI publication: TR-304, 17/2/2009, pp22.

Minnis, P., K. N. Liou, and Y. Takano, 1993: Inference of Cirrus Cloud Properties Using Satellite-observed Visible and Infrared Radiances. Part I: Parameterization of Radiance Fields. *J. Atmos. Sci.*, **50**, 1279–1304.

Nakajima, T., and M. D. King, 1990: Determination of the Optical Thickness and Effective Particle Radius of Clouds from Reflected Solar Radiation Measurements. Part 1: Theory. *J. Atmos. Sci.*, **47**, 1878–1893.

Nakajima, T. Y., and T. Nakajima, 1995: Wide-Area Determination of Cloud Microphysical Properties from NOAA AVHRR Measurements for FIRE and ASTEX regions. *J. Atmos. Sci.*, **52**, 4043 – 4059.

Oreopoulos, L., and R. Davies, 1998: Plane parallel albedo biases from satellite observations. part I: Dependence on resolution and other factors: *J. Climate*, **11**, 919–932.

<i>EUMETSAT Satellite Application Facility to NoWCASTing & Very Short Range Forecasting</i>	Algorithm Theoretical Basis Document for Cloud Micro Physics of the NWC/PPS	Code: NWC/CDOP3/PPS/SMHI/SCI/ATBD/CMIC Issue: 3.1.0 Date: 01 September 2022 File: NWC-CDOP3-PPS-SMHI-SCI-ATBD-CMIC_v3_1_0 Page: 15/49
---	---	---

Pavolonis, M. J. and A. K. Heidinger, 2004: Daytime cloud overlap detection from AVHRR and VIIRS, *J. Appl. Meteorol.*, **43**, 762-778.

Pavolonis, M. J., A. K. Heidinger, and T. Uttal, 2005: Daytime global cloud typing from AVHRR and VIIRS: Algorithm description, validation, and comparison, *J. Appl. Meteorol.*, **44**, 804-826.

Platnick, S., 2001: A superposition technique for deriving mean photon scattering statistics in plane-parallel cloudy atmospheres, *J. Quant. Spectrosc. Radiat. Transfer*, **68**, 57-73.

Platnick, S., Meyer, K. G., D., K. M., Wind, G., Amarasinghe, N., Marchant, B., Arnold, G. T., Zhang, Z., Hubanks, P. A., Holz, R. E., Yang, P., Ridgway, W. L., and Riedi, J., 2017: The MODIS Cloud Optical and Microphysical Products: Collection 6 Updates and Examples From Terra and Aqua, *IEEE T. Geosci. Remote*, **55**, 502–525, doi: 10.1109/TGRS.2016.2610522.

Rodgers, C.D., 2000: *Inverse methods for atmospheric sounding: theory and practice*, World Scientific, Hackensack, NJ, USA, 238 pp.

Roebeling, R. A., 2008: Cloud Physical Properties Retrieval for Climate Studies using SEVIRI and AVHRR data, PhD Thesis, Wageningen University, The Netherlands, 160pp. Available from <http://www.knmi.nl/publications>.

Roebeling, R. A., A. Berk, A. J. Feijt, W. Frerichs, D. Jolivet, A. Macke, and P. Stammes, 2005: Sensitivity of cloud property retrievals to differences in narrow band radiative transfer simulations, KNMI Scientific Report, WR 2005-02, Royal Netherlands Meteorological Institute, De Bilt, the Netherlands, 27 pp. Available from <http://www.knmi.nl/publications>.

Roebeling, R. A., A. J. Feijt, and P. Stammes, 2006: Cloud property retrievals for climate monitoring: implications of differences between SEVIRI on METEOSAT-8 and AVHRR on NOAA-17, *J. Geophys. Res.*, **111**, D20210, doi:10.1029/2005JD006990.

Rosenfeld, D., E. Cattani, S. Melani, and V. Levizzani, 2004: Considerations on daylight operation of 1.6- versus 3.8- μ m channel on NOAA and Metop satellites. *B. Am. Meteorol. Soc.*, **85**, 873–881.

Rossow, W.B., and R.A. Schiffer, 1999: Advances in understanding clouds from ISCCP. *B. Am. Meteorol. Soc.*, **80**, 2261-2287.

Saunders, R., Hocking, J., Turner, E., Rayer, P., Rundle, D., Brunel, P., Vidot, J., Roquet, P., Matricardi, M., Geer, A., Bormann, N., and Lupu, C., 2018: An update on the RTTOV fast radiative transfer model (currently at version 12), *Geosci. Model Dev.*, **11**, 2717-2737, <https://doi.org/10.5194/gmd-11-2717-2018>

Seemann, S.W., E. E. Borbas, R. O. Knuteson, G. R. Stephenson, H.-L. Huang, 2008: Development of a Global Infrared Land Surface Emissivity Database for Application to Clear Sky Sounding Retrievals from Multi-spectral Satellite Radiance Measurements, *J. Appl. Meteorol. Clim.*, **47**, 108-123.

Seethala, C. and A. Horvath, 2010: Global assessment of AMSR-E and MODIS cloud liquid water path retrievals in warm oceanic clouds, *J. Geophys. Res.*, **115**, D13202, doi:10.1029/2009JD012662.

Segelstein, D., 1981: The complex refractive index of water, M.Sc. Thesis, Univ. of Missouri, Kansas City.

Schumann, U., B. Mayer, K. Gierens, S. Unterstrasser, P. Jessberger, A. Petzold, C. Voigt, J.-F. Gayet, 2011: Effective radius of ice particles in cirrus and contrails. *J. Atmos. Sci.*, **68**, 300–321, doi:10.1175/2010JAS3562.1.

Stammes, P., 2001: Spectral radiance modeling in the UV-Visible range. IRS 2000: Current problems in Atmospheric Radiation, edited by W.L. Smith and Y.M. Timofeyev, pp 385-388, A. Deepak Publ., Hampton, Va.

<i>EUMETSAT Satellite Application Facility to NoWCASTing & Very Short Range Forecasting</i>	Algorithm Theoretical Basis Document for Cloud Micro Physics of the NWC/PPS	Code: NWC/CDOP3/PPS/SMHI/SCI/ATBD/CMIC Issue: 3.1.0 Date: 01 September 2022 File: NWC-CDOP3-PPS-SMHI-SCI-ATBD-CMIC_v3_1_0 Page: 16/49
---	---	---

Stamnes, K., S. C Tsay, W. Wiscombe, and K Jayaweera, 1988: Numerically stable algorithm for discrete ordinate method radiative transfer in multiple scattering and emitting layered media. *Appl. Optics*, **27**, 2502-2509.

Stephens, G. L. and C. D. Kummerow, 2007: The Remote Sensing of Clouds and Precipitation from Space: A Review. *J. Atmos. Sci.*, **64**, 3742–3765.

Sun, Q., Wang, Z., Li, Z., Erb, A., and Schaaf, C. L. B., 2017: Evaluation of the global MODIS 30 arc-second spatially and temporally complete snow-free land surface albedo and reflectance anisotropy dataset. *Int. J. Appl. Earth Obs.*, 58, 36-49, doi: 10.1016/j.jag.2017.01.011.

Van der A, R. J., Allaart, M. A. F., and Eskes, H. J., 2010: Multi sensor reanalysis of total ozone, *Atmos. Chem. Phys.*, **10**, 11277–11294, doi:10.5194/acp-10-11277-2010.

Warren, S. G. and R. E. Brandt, 2008: Optical constants of ice from the ultraviolet to the microwave: A revised compilation. *J. Geophys. Res.*, **113**, D14220, doi:10.1029/2007JD009744.

Watts, P. D., C. T. Mutlow, A. J. Baran, and A. M. Zavody, 1998: Study on Cloud Properties derived from Meteosat Second Generation Observations, Final Report, EUMETSAT ITT no. 97/181.

Wilcox, E. M., Harshvardhan, and S. Platnick, 2009: Estimate of the impact of absorbing aerosol over cloud on the MODIS retrievals of cloud optical thickness and effective radius using two independent retrievals of liquid water path, *J. Geophys. Res.*, **114**, D05210, doi:10.1029/2008JD010589.

Wolters, E. L. A., H. M. Deneke, B. J. J. M. van den Hurk, J. F. Meirink, and R. A. Roebeling, 2010: Broken and inhomogeneous cloud impact on satellite cloud particle effective radius and cloud-phase retrievals, *J. Geophys. Res.*, **115**, doi:10.1029/2009JD012205.

Wolters, E. L. A., R. A. Roebeling, and P. Stamnes, 2006: Cloud reflectance calculations using DAK: study on required integration points, KNMI Technical Report, TR-292, Royal Netherlands Meteorological Institute, De Bilt, The Netherlands, 17 pp. Available from <http://www.knmi.nl/publications>.

Yang, P., L. Bi, B. A. Baum, K.-N. Liou, G. W. Kattawar, M. I. Mishchenko, and B. Cole, 2013: Spectrally consistent scattering, absorption, and polarization properties of atmospheric ice crystals at wavelengths from 0.2 to 100 μm , *J. Atmos. Sci.*, **70**, 330-347, doi:10.1175/JAS-D-12-039.1.

Zhang, Z., A. S. Ackerman, G. Feingold, S. Platnick, R. Pincus, and H. Xue, 2012: Effects of cloud horizontal inhomogeneity and drizzle on remote sensing of cloud droplet effective radius: Case studies based on large-eddy simulations, *J. Geophys. Res.*, **117**, D19208, doi:10.1029/2012JD017655.

Zhang, Z., and S. Platnick, 2011: An assessment of differences between cloud effective particle radius retrievals for marine water clouds from three MODIS spectral bands, *J. Geophys. Res.*, **116**, D20215, doi:10.1029/2011JD016216.

Zhang, Z., P. Yang, G. Kattawar, Riedi, J., Labonnote, L. C., Baum, B. A., Platnick, S., and Huang, H.-L., 2009: Influence of ice particle model on satellite ice cloud retrieval: lessons learned from MODIS and POLDER cloud product comparison, *Atmos. Chem. Phys.*, **9**, 7115-7129, doi: 10.5194/acp-9-7115-2009.

Zinner, T., G. Wind, S. Platnick, and A.S. Ackerman, 2010: Testing remote sensing on artificial observations: impact of drizzle and 3-D cloud structure on effective radius retrievals, *Atmos. Chem. Phys.*, **10**, 9535-9549, doi:10.5194/acp-10-9535-2010.

<i>EUMETSAT Satellite Application Facility to NoWCasting & Very Short Range Forecasting</i>	Algorithm Theoretical Basis Document for Cloud Micro Physics of the NWC/PPS	Code: NWC/CDOP3/PPS/SMHI/SCI/ATBD/CMIC Issue: 3.1.0 Date: 01 September 2022 File: NWC-CDOP3-PPS-SMHI-SCI-ATBD-CMIC_v3_1_0 Page: 17/49
---	---	---

1.5. DOCUMENT OVERVIEW

The set-up of this document is as follows. In Section 3 a short overview of the retrieval algorithms is presented. Section 4 gives a detailed description of the retrieval algorithms, consisting of the relevant underlying physics (Section 4.1), the radiative transfer modelling (Section 4.2), the implementation of the retrieval scheme (Section 4.3), the error budget of the retrieved products (Section 4.4), and the practical application of the algorithms (Section 4.5). Finally, assumptions and limitations are discussed in Section 5.

1.6. SCIENTIFIC UPDATES SINCE PPS VERSION 2018

Since PPS Version 2018, for the v2018-patches several updates to the CPP software (CMIC product) have been implemented. The most important ones, which applies both for PPS v2021 and vEPSSG, are:

- The capability to process MERSI-2 observations has been added.
- The option to use the new PPS product Cloud Probability has been added, instead of the Cloud Mask (configurable).
- New by-products Cloud Droplet Number Concentration (CDNC) and Cloud Geometrical Thickness (CGT) for liquid clouds have been introduced.
- The uncertainty estimates of all products have been revised and extended.
- The radiative transfer look-up tables have been modified based on different choices for ice particle habits and size distribution and water droplet size distribution width.
- Several smaller algorithm updates have been implemented.

For PPS vEPSSG: (This is also included in PPS v2021.2, as demonstrational features.)

- Data from METImage (EPS-SG) can be processed. (As demonstrational in the beta release vEPSSG-SAFbeta3 and in v2021.2.) Obviously, this is not yet validated for the vEPSSG-beta releases.
- Start using a number of additional channels, which are not AVHRR-heritage, for METImage and VIIRS. These channels are mainly exploited for an improved retrievals of cloud thermodynamic phase and particle effective radius, impacting the liquid and ice water path products. For vEPSSG-SAFbeta3 is channel 2.2 μ m used (configurable), more channels to be added after launch. (For v2021.2 this is also available, but in the default configuration it is turned off.)

2. INTRODUCTION TO THE SAFNWC/PPS CLOUD MICROPHYSICS PRODUCT

This SAFNWC Algorithm Theoretical Basis Document (ATBD) provides detailed information on the retrieval algorithm deriving cloud microphysics (CMIC) products from VIS-NIR-IR satellite imagers. The algorithm retrieves cloud-top phase and liquid water path as official products. Cloud optical thickness, cloud particle effective radius, ice water path, extended cloud-top phase, liquid cloud droplet number concentration and liquid cloud geometrical thickness are derived as additional products.

Table 4: Overview of SAF products covered in this ATBD.

Cloud property	Explanation	Status in NWCSAF/PPS
CPH	Cloud-top thermodynamic phase	Official product
LWP	cloud liquid water path	Official product
CPH_extended	Cloud-top thermodynamic phase, more classes than in CPH	Additional product
IWP	Cloud ice water path	Additional product
COT	cloud optical thickness	Additional product
CRE	Cloud particle effective radius	Additional product
CDNC	Liquid Cloud Droplet Number Concentration	Additional product
CGT	Liquid Cloud Geometrical Thickness	Additional product

Further details about this cloud physical property software can be found in the product user manual ([RD.3]). The requirements for the SAFNWC/PPS CMIC products can be found in [AD.1]. The quality of the official products, CPH and LWP, is discussed in the validation report [RD.4].

The software is used by CM-SAF to generate climate data records of cloud properties. Their AVHRR-based climate record named CLARA-A2 (Karlsson et al., 2017), including the cloud physical properties (cloud micro physics), was extensively validated in [RD.2]. The algorithm description in this ATBD is originally based on Roebeling (2008) and Roebeling et al. (2006), but contains a range of modifications and improvements implemented since then.

The cloud micro physics retrieval algorithm requires a cloud mask and cloud-top height and temperature as input. The SAFNWC/PPS algorithms for these products are described in [RD.5] and [RD.6].

2.1. REQUIREMENTS

The requirements for the SAFNWC/PPS products are described in the Product Requirements Document [AD.1]. In Table 5 and Table 6 is given a summary of the requirement specific for the cloud micro physics product.

Table 5 Accuracy requirements for CMIC Cloud Phase

	Water POD	Water FAR	Ice POD	Ice FAR
Threshold accuracy	70%	35%	60%	35%
Target accuracy	80%	20%	80%	20%
Optimal accuracy	90%	10%	90%	10%

Table 6 Accuracy requirements for CMIC Liquid Water Path

	RMS	Bias
Threshold accuracy	100 g/m ²	20 g/m ²
Target accuracy	50 g/m ²	10 g/m ²
Optimal accuracy	20 g/m ²	5 g/m ²

<i>EUMETSAT Satellite Application Facility to NoWCasting & Very Short Range Forecasting</i>	Algorithm Theoretical Basis Document for Cloud Micro Physics of the NWC/PPS	Code: NWC/CDOP3/PPS/SMHI/SCI/ATBD/CMIC Issue: 3.1.0 Date: 01 September 2022 File: NWC-CDOP3-PPS-SMHI-SCI-ATBD-CMIC_v3.1_0 Page: 20/49
---	---	---

3. ALGORITHM OVERVIEW

The CMIC (cloud micro physics) algorithm consists of two main parts. First, the cloud-top thermodynamic phase (CPH) is determined from a cloud typing approach following Pavolonis and Heidinger (2004) and Pavolonis et al. (2005). This cloud phase algorithm consists of a series of spectral tests applied to infrared brightness temperatures. It has a nighttime branch as well as a daytime branch in which shortwave reflectances are considered in addition.

The algorithm then proceeds with retrieving cloud optical thickness (COT or τ) and cloud particle effective radius (CRE or r_e), during daytime given the thermodynamic phase determined before. This retrieval scheme was developed at KNMI, first described in Roebeling et al. (2006), and is based on earlier methods that retrieve cloud optical thickness and cloud particle effective radius from satellite radiances at wavelengths in the non-absorbing visible and the moderately absorbing solar infrared part of the spectrum (Nakajima and King 1990; Nakajima and Nakajima 1995; Watts et al. 1998). Liquid and ice water path (LWP/IWP) as well as cloud droplet number concentration (CDNC) and cloud geometrical thickness (CGT) for liquid clouds are derived from COT and CRE.

4. ALGORITHM DESCRIPTION

4.1. THEORETICAL DESCRIPTION

The principle of the CMIC retrieval algorithm is that the reflectance of clouds at a non-absorbing wavelength in the visible region (VIS: 0.6 or 0.8 μm) is strongly related to the optical thickness and has little dependence on particle size, whereas the reflectance of clouds at an absorbing wavelength in the near-infrared region (NIR: e.g., 1.6, 2.2 or 3.8 μm) is primarily related to particle effective radius. This feature allows the retrieval of COT and CRE from two channels of a passive imager. Moreover, Figure 1 shows that the imaginary parts of the refractive indices of water and ice, which are a measure for absorption, differ. For example, around 1.6 and 3.8 μm ice particles are more absorbing than water droplets. This feature, together with a series of spectral tests on the thermal infrared (IR) window channels is used to retrieve (daytime) cloud-top thermodynamic phase.

The cloud optical thickness τ is defined at 0.6 μm under the assumption of a plane parallel atmosphere with reference to a vertical transect. The particle effective radius r_e is the relevant quantity for radiative scattering, and is given by the ratio of the mean particle volume to the mean projected cross-sectional area A (e.g., Schumann et al., 2011):

$$r_e = \frac{3V}{4A} \quad (1)$$

In case of a collection of spherical water droplets, this can be rewritten to:

$$r_e = \frac{\int_0^\infty r^3 n(r) dr}{\int_0^\infty r^2 n(r) dr} \quad (2)$$

where r is the droplet radius, and $n(r) dr$ is the number of particles per unit volume with radius between r and $r+dr$. Given the relatively small penetration depth into the cloud of photons at

<i>EUMETSAT Satellite Application Facility to NoWCASTing & Very Short Range Forecasting</i>	Algorithm Theoretical Basis Document for Cloud Micro Physics of the NWC/PPS	Code: NWC/CDOP3/PPS/SMHI/SCI/ATBD/CMIC Issue: 3.1.0 Date: 01 September 2022 File: NWC-CDOP3-PPS-SMHI-SCI-ATBD-CMIC_v3_1_0 Page: 21/49
---	---	---

shortwave-infrared wavelengths, the retrieved effective radius reflects conditions near the cloud top.

The liquid water path (LWP or W) is calculated from τ and r_e assuming vertically homogenous liquid water content (LWC):

$$LWP = \frac{2}{3} \frac{2}{Q_e} \rho_l \tau r_e \quad (3)$$

where $\rho_l = 1.0 \times 10^3 \text{ kg m}^{-3}$ is the density of water and Q_e is the extinction efficiency at $0.6 \mu\text{m}$, which can be approximated by its asymptotic value of 2 for cloud droplets that are large compared to visible wavelengths.

The liquid cloud droplet number concentration (CDNC or N_d) and liquid cloud geometrical thickness (CGT or H_g) can be determined from the retrieved τ and r_e following a model termed Idealized Stratiform Boundary Layer Cloud (ISBLC) by Bennartz and Rausch (2017). It assumes a linearly increasing liquid water content (LWC) with height and a vertically constant CDNC. This model yields the following relations (see also Grosvenor et al., 2018):

$$H_g = \frac{2}{3} \left(\frac{5 \rho_l \tau r_e}{Q_e f_{ad} c_w} \right)^{\frac{1}{2}} \quad (4)$$

$$N_d = \frac{1}{2\pi k} \left(\frac{5 f_{ad} c_w \tau}{Q_e \rho_l r_e^5} \right)^{\frac{1}{2}} \quad (5)$$

where k is the third power of the ratio between volume mean radius and effective radius, which is set to 0.8, and c_w is the rate of increase in LWC with height for moist adiabatic ascent in kg m^{-4} (which is multiplied by the so-called adiabatic factor f_{ad} , set to 0.8, to obtain the actual rate of increase in LWC with height):

$$c_w = \rho_a \frac{c_p}{L_v} (\Gamma_m(T, P) - \Gamma_d) \quad (6)$$

where ρ_a is the air density, c_p is the specific heat of dry air at constant pressure, L_v is the latent heat of vaporization, and Γ_d and Γ_m are the dry and moist adiabatic lapse rates, respectively. The latter is a weak function of temperature and pressure, for which their values at the cloud top are taken.

Finally, Ice Water Path (IWP) is computed analogously to LWP assuming vertically homogeneous ice water content (ICW), leading to:

$$IWP = \frac{2}{3} \frac{2}{Q_e} \rho_i \tau r_e \quad (7)$$

where $\rho_i = 0.93 \times 10^3 \text{ kg m}^{-3}$ is the density of ice.

It should be noted that two different assumptions for the vertical profile of liquid water clouds have been employed. It was decided to adopt vertically homogeneous r_e and LWC in Eq. (3) for the calculation of LWP, consistently with the assumptions made in the radiative transfer simulations (see Section 4.2) and with those for ice clouds in Eq. (7). In contrast, the ISBLC model used for the calculation of CDNC and CGT is based on linearly increasing r_e and LWC with height, where r_e is assumed to be the effective radius at the top of the cloud. In that case, LWP is given by the same relation as in Eq. (3) but with the factor $2/3$ replaced by $5/9$, as

outlined, for example, in Borg and Bennartz (2007). Inserting this formulation for LWP in Eqs. (1) and (2) of Bennartz and Rausch (2017) and including the adiabatic factor f_{ad} yields our Eqs. (4) and (5), respectively.

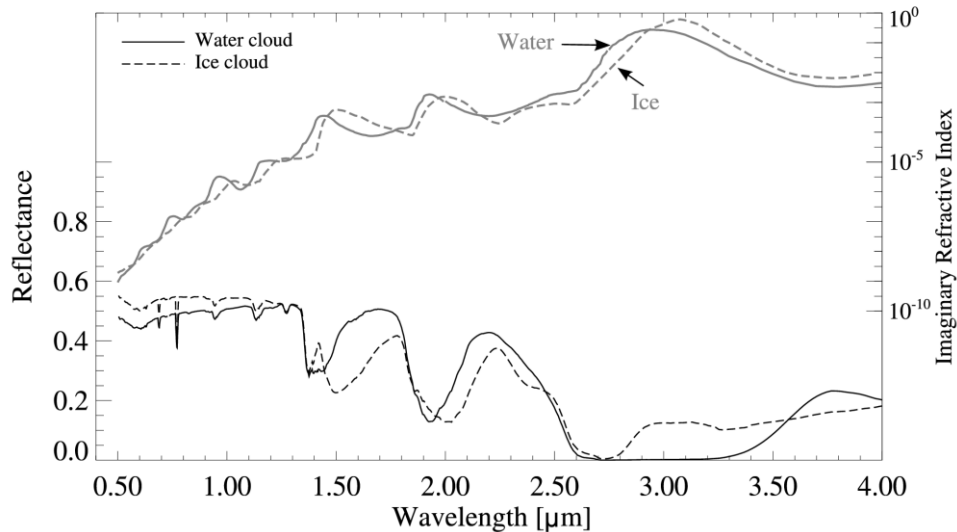


Figure 1 Simulated top-of-atmosphere (TOA) reflectance spectra for a stratocumulus (water) cloud and a cirrus (ice) cloud, and the imaginary part of the index of refraction of water and ice. The simulations were made with the MODerate spectral resolution atmospheric TRANsmittance and radiance code (MODTRAN) at $\theta_0 = 45^\circ$, $\theta = 0^\circ$ and $\phi = 0^\circ$. The reflectances are plotted as black lines, while the refractive indices are plotted as gray lines.

4.2. RADIATIVE TRANSFER

The usage of channel 2.2 μm is configurable, and obviously only relevant for instruments having that channel, i.e. METImage and VIIRS.

The CMIC algorithm compares satellite observed reflectances at visible and near-infrared wavelengths to look-up tables (LUTs) of simulated reflectances for given cloud optical thicknesses, particle sizes and surface albedos for water and ice clouds (Watts et al. 1998; Jolivet and Feijt 2003). The Doubling Adding KNMI (DAK) radiative transfer model (RTM) has been used to generate the LUTs of simulated cloud reflectances. DAK has been developed for line-by-line or monochromatic multiple scattering calculations at UV, visible and near infrared wavelengths in a horizontally homogeneous cloudy atmosphere using the doubling-adding method (De Haan et al. 1987; Stammes 2001). DAK first calculates the reflection and transmission of an optically thin layer, in which no more than two scattering events may occur. Thanks to this restriction the radiative transfer equation can be solved analytically. Next, the reflection and transmission of two identical layers on top of each other can be obtained by computing successive reflections back and forth between the layers. This doubling procedure is continued until the actual optical thickness of the cloud is reached. The DAK model includes polarization. A pseudo-spherical correction is used as in Caudill et al. (1997). This correction accounts for attenuation of the solar beam as in a spherical atmosphere, while higher-order scattering is calculated for a plane-parallel atmosphere. DAK has been selected because it is the KNMI in-house shortwave RTM, and there is ample hands-on experience with this RTM at KNMI. Furthermore,

<i>EUMETSAT Satellite Application Facility to NoWCasting & Very Short Range Forecasting</i>	Algorithm Theoretical Basis Document for Cloud Micro Physics of the NWC/PPS	Code: NWC/CDOP3/PPS/SMHI/SCI/ATBD/CMIC Issue: 3.1.0 Date: 01 September 2022 File: NWC-CDOP3-PPS-SMHI-SCI-ATBD-CMIC_v3_1_0 Page: 23/49
---	---	---

comparisons with other RTMs have been performed, showing generally trustworthy results for DAK (Roebeling et al., 2005, see also Section 4.4).

Clouds are assumed to be plane-parallel and embedded in a multi-layered Rayleigh scattering atmosphere. The particles of water clouds are assumed to be spherical droplets with effective radii between 3 and 34 μm and an effective variance of 0.1. The latter value replaces an effective variance of 0.15 used in earlier CPP versions based on the findings of Benas et al. (2019) and references therein. Scattering properties were calculated with Mie theory.

For ice clouds, severely roughened compact aggregates of eight solid columns has been adopted (Yang et al., 2013; Baum et al., 2011), as is also used in the MODIS Collection 6 (MOD06 C6) algorithms (Platnick et al., 2017). This aggregate solid column habit replaces the imperfect (i.e. roughened), randomly oriented, hexagonal ice crystals in monodisperse size distributions (Hess et al., 1998) which were used in earlier CPP versions. Effective radii between 5 and 60 μm are considered and size distributions have an effective variance of 0.1. The scattering properties were obtained from Baum (2014).

Scattering phase functions of water droplets and ice crystals are compared in Figure 2. For water droplets a strong reduction in sideways scattering is observed as well as enhanced scattering at the rainbow angle and in backscatter direction. Smooth ice crystals tend to yield distinct halo features and a strong backscatter peak. In contrast, roughened crystals show virtually featureless phase functions, and also yield considerably lower asymmetry parameters compared to smooth crystals (Zhang et al., 2009). The imperfect hexagonal crystals and the aggregate solid columns yield quite similar phase functions, although there are differences, which are further illustrated in Figure 3 in terms of the asymmetry parameter g , and the single scattering albedo ω_0 . Changes in these properties have implications for the τ and r_e retrievals (see Platnick et al., 2017 for a discussion). The asymmetry parameter has decreased somewhat at all wavelengths with the new ice crystal model. A reduction in g at 0.6 μm leads to smaller retrieved τ because the quantity $\tau(1 - \omega_0 g)$ has been found to be invariant. The single scattering albedo has increased with the new ice habit. This lower absorption leads to higher simulated cloud reflectances at the absorbing wavelengths and thus larger retrieved r_e .

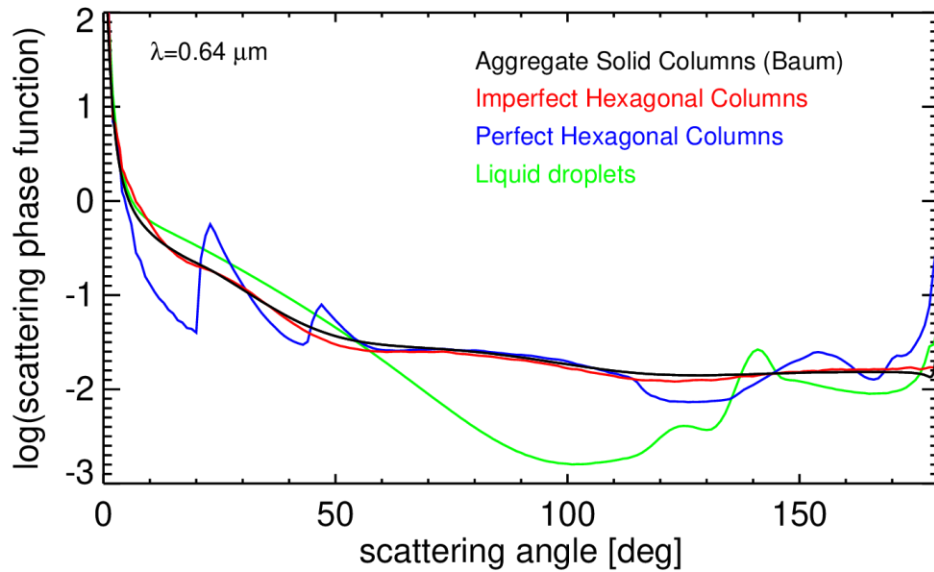


Figure 2: Comparison between scattering phase functions of the severely roughened aggregate solid column habit, imperfect (roughened) hexagons, perfect (smooth) hexagons, and water droplets. The wavelength is $0.64 \mu\text{m}$ and the effective radii are $12 \mu\text{m}$ for the water droplets and $10 \mu\text{m}$ for the ice crystals.

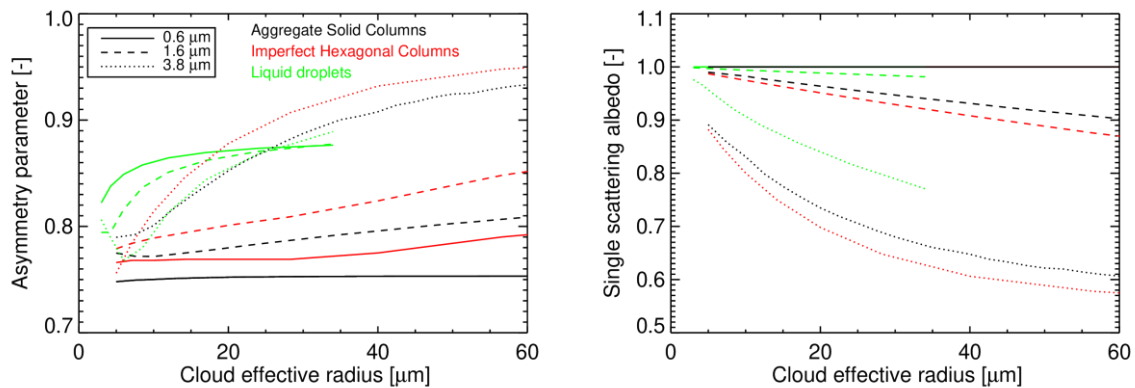


Figure 3: Asymmetry parameter (left) and single scattering albedo (right) as a function of cloud particle effective radius for the aggregate solid column and imperfect hexagon habits as well as liquid cloud droplets. Results are shown for three wavelengths: 0.6 , 1.6 and $3.8 \mu\text{m}$.

Figure 4 shows an example of DAK calculations of 0.6 and $1.6/2.2/3.8 \mu\text{m}$ reflectances as function of τ and r_e for water droplets and ice crystals. The figure illustrates that for optically thick clouds lines of equal τ and r_e are nearly orthogonal, meaning that the 0.6 and $1.6/2.2/3.8 \mu\text{m}$ reflectances contain independent information on τ and r_e , respectively. This is not the case for optically thin clouds. Moreover, for these clouds, the lines of different r_e are very close together, implying that the retrieval of particle size is inherently uncertain. The three NIR channels behave qualitatively similar but have different properties: broadly speaking the dynamical range in reflectance decreases towards longer wavelengths due to stronger absorption (Figure 1), while at

the same time the lines of equal τ and r_e become orthogonal. Further, it is evident that ice clouds have lower 1.6- μm and 3.8- μm reflectances than water clouds, which is a consequence of the stronger absorption of ice particles compared to water droplets at these wavelengths (see Figure 1), whereas the reflectance of water and ice clouds is much more similar at 2.2 μm .

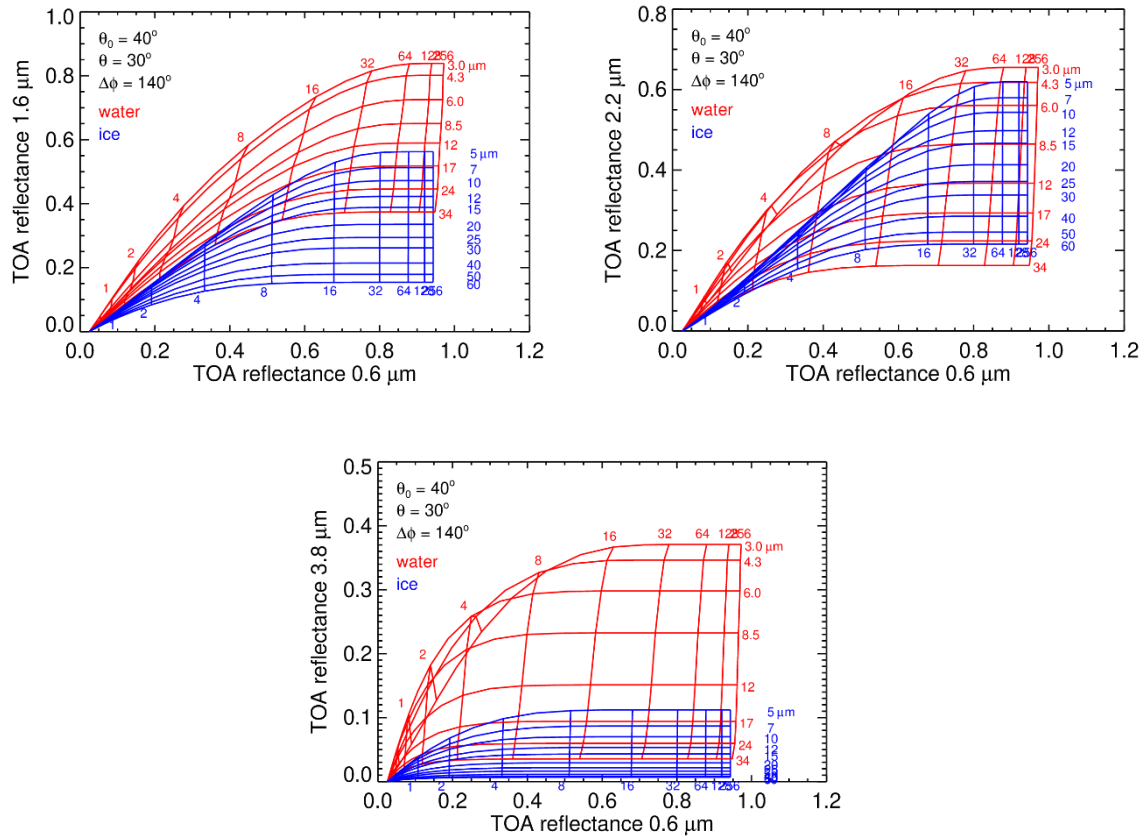


Figure 4 DAK calculations of TOA reflectance at 0.6 μm versus 1.6 μm (top left), 2.2 μm (top right) and 3.8 μm (bottom) for clouds consisting of spherical water droplets (red curves) and roughened, aggregate solid ice columns (blue curves). The reflectances have been calculated over a black surface (albedo = 0). Solar and satellite angles are indicated in the plots. The vertically oriented lines represent lines of equal cloud optical thickness, while the horizontally oriented lines represent lines of equal particle size. Values of optical thickness and cloud particle effective radius are indicated in the plot. Note the different scaling of the vertical axis in both panels.

Table 7 Properties of the cloudy atmosphere that are used for the radiative transfer calculations to generate the LUTs.

Parameter	Settings
Vertical profiles of pressure, temperature, and ozone	Midlatitude summer ^{a)}
Aerosol model	None
Cloud height	Water clouds: 1000-2000 m; Ice clouds: 5000-6000 m
Solar zenith angle (θ_0) ^{b)}	0 - 84.3° (73 Gaussian points in $\mu_0 = \cos(\theta_0)$)
Viewing zenith angle (θ) ^{b)}	Same as θ_0
Relative azimuth angle (ϕ) ^{b)}	0 - 180° (equidistant, 91 points)

<i>EUMETSAT Satellite Application Facility to NoWCasting & Very Short Range Forecasting</i>	Algorithm Theoretical Basis Document for Cloud Micro Physics of the NWC/PPS	Code: NWC/CDOP3/PPS/SMHI/SCI/ATBD/CMIC Issue: 3.1.0 Date: 01 September 2022 File: NWC-CDOP3-PPS-SMHI-SCI-ATBD-CMIC_v3_1_0 Page: 26/49
---	---	---

Cloud optical thickness	0 – 256 (equidistant in $\log(\tau)$, 22 points)	
	water clouds	ice clouds
Cloud particle type	Spherical water droplet	Roughened aggregate solid columns
Cloud particle size	3–34 μm equidistant in $\log(r_e)$, 8 points	[5, 7.5, 10, 12.5, 15, 20, 25, 30, 40, 50, 60 μm] (11 points)
Liquid / Ice water path	0 – 4,836 g m^{-2}	0 – 9,523 g m^{-2}
Size distribution	Two-parameter gamma	Two-parameter gamma
Effective variance (v_e)	0.1	0.1
Complex refractive index	Segelstein (1981)	Warren and Brandt (2008)

^{a)} The midlatitude summer (MLS) atmosphere model was taken from Anderson et al. (1986). The choice of the temperature and pressure profile has a marginal impact on the LUT, namely only through Rayleigh scattering. Deviations from the MLS total column ozone are taken into account in the atmospheric correction procedure, see Eq. (9).

^{b)} The chosen distributions of angles are motivated in Wolters et al. (2006).

Table 7 summarizes the governing characteristics of the cloudy atmosphere, together with information about intervals of cloud properties and viewing geometries used in the DAK simulations to generate the LUT. The DAK simulations were done for a black surface. The TOA reflectance $R(\alpha_s)$ over a surface with reflectance α_s is computed using (Chandrasekhar, 1960):

$$R(\alpha_s) = R(\alpha_s = 0) + \frac{\alpha_s t_c(\theta_0) t_c(\theta)}{1 - \alpha_s \alpha_a} \quad (8)$$

Here, $t_c(\theta_0)$ and $t_c(\theta)$ are the cloud transmissivities at the solar and viewing zenith angles, respectively, and α_a is the hemispherical sky albedo for upwelling, isotropic radiation. The required parameters are determined from two additional DAK calculations with surface reflectance values of 0.5 and 1.0.

The DAK calculations concern monochromatic radiative transfer at a wavelength close to the centre of the respective satellite imager narrowbands. These calculations include Rayleigh scattering by air molecules and absorption by ozone at this wavelength, but neglect absorption by other atmospheric gases. Before the reflectance simulated by DAK can be compared to an observed reflectance, the absorption by atmospheric gases in the band has to be taken into account. This so-called atmospheric correction has been implemented based on MODTRAN4.2 (Berk et al. 2000) radiative transfer simulations. The atmosphere-corrected TOA reflectance ($R_{\text{atm.corr.}}$) is calculated as:

$$R_{\text{atm.corr.}} = R t_{a,ac}(\theta_0, H_c, WVP, TCO) t_{a,ac}(\theta, H_c, WVP, TCO) \quad (9)$$

where $t_{a,ac}$ is the above-cloud atmospheric transmissivity. Fixed (MLS) vertical profiles of water vapour and ozone are assumed, so that $t_{a,ac}$ becomes a function of the viewing or solar zenith angle, the cloud top height (H_c), water vapor path (WVP) and total column ozone (TCO). Absorption by trace gases within and below the cloud is neglected. The two-way transmissivity, i.e. the product of the two transmissivities in Eq. (9), is a function of the geometrical air mass factor ($\text{AMF} = 1/\mu_0 + 1/\mu$). This two-way transmissivity is in practice simulated by MODTRAN using a Lambertian surface, with arbitrary reflectance, placed at the cloud top height, and stored in a LUT with dimensions AMF, H_c , WVP, and TCO. An indication of the magnitude of the atmospheric correction is given in Table 8. Note that the atmospheric correction depends on the exact spectral response of the specific instrument channels.

Table 8 Typical magnitude of atmospheric correction, expressed as 1 minus the two-way transmissivity, in %. The numbers have been calculated for a reference atmosphere ($H_c = 2 \text{ km}$,

AMF = 2, TCO = 332 DU, and WVP = 30 kg m⁻²), based on the NOAA-15 AVHRR spectral response, and for individual absorbing gases as well as for all gases together.

Gas	Channel 1	Channel 3a	Channel 3b
H ₂ O	0.6 %	0.2 %	11.9 %
O ₃	0.7 %	-	-
O ₂	0.1 %	-	-
CO ₂		3.1 %	0.2 %
CH ₄		0.1 %	3.7 %
N ₂ O			1.6 %
N ₂ -continuum			0.7 %
All gases	1.5 %	3.4 %	17.6 %

More details on the implementation of atmospheric correction and the effect on retrieved cloud properties can be found in Meirink et al. (2009).

Whereas at 1.6 and 2.2 μm reflected sunlight is the only significant component of the measured TOA radiance, at 3.8 μm thermal emission by the surface, atmosphere and clouds provides a non-negligible contribution. Thermal emission is expressed as a reflectance (R_e), and calculated as the sum of contributions from surface ($R_{e,s}$) and cloud ($R_{e,c}$) following Nakajima and Nakajima (1995):

$$R_e = R_{e,s} + R_{e,c} = \left(\varepsilon_s B_\lambda(T_s) t_a(\theta) t_c(\theta) + \varepsilon_c B_\lambda(T_c) t_{a,ac}(\theta) \right) \frac{\pi}{\mu_0 F_{0,\lambda}}. \quad (10)$$

where ε_s is the surface emissivity, T_s and T_c are the surface and cloud-top temperatures, respectively, $B_\lambda(T)$ is the Planck function at temperature T and wavelength λ ($= 3.8 \mu\text{m}$), $F_{0,\lambda}$ is the extraterrestrial solar flux at wavelength λ , and ε_c is the cloud emissivity approximated as:

$$\varepsilon_c = 1 - t_c(\theta) - R(\theta_0, \theta, \varphi). \quad (11)$$

ε_c is a function of τ and r_e through the cloud transmissivity t_c and reflectivity R . The retrieval procedure is the same as for the shorter-wavelength channels with the observed 3.8- μm radiance converted to a reflectance which is compared with the sum of simulated reflected sunlight and thermal emission.

4.3. RETRIEVAL SCHEME

The CMIC retrieval scheme consists of two parts. The first part is the retrieval of an extended cloud phase, and is described in Section 4.3.1. This extended phase is then reduced to two categories: liquid and ice. The second part is the retrieval of cloud optical properties (optical thickness and cloud particle effective radius) for the retrieved phase. This is further described in Section 4.3.2.

<i>EUMETSAT Satellite Application Facility to NoWCasting & Very Short Range Forecasting</i>	Algorithm Theoretical Basis Document for Cloud Micro Physics of the NWC/PPS	Code: NWC/CDOP3/PPS/SMHI/SCI/ATBD/CMIC Issue: 3.1.0 Date: 01 September 2022 File: NWC-CDOP3-PPS-SMHI-SCI-ATBD-CMIC_v3_1_0 Page: 28/49
---	---	---

4.3.1. Cloud phase

The capability of detecting cloud phase depends on the spectral information available.. The algorithm described in Section 4.3.1.1 specifically targets the AVHRR channels, and can also be run using similar channels on more recent imagers. As outlined in Section 4.3.1.2, an improved algorithm targeting the wider range of channels available on METImage will be considered for day-2 (TBD03).

The AVHRR-heritage algorithm determines an extended cloud phase from one of the following categories: fog, liquid, supercooled, opaque ice, cirrus, overlap (ice above liquid), and overshooting (only for the METImage algorithm) as described in the next subsection.

Subsequently, the consistency of the retrieved extended cloud phase with the cloud-top temperature is checked. Very cold clouds are not allowed to be liquid, and warm clouds are not allowed to be ice. Concretely, if the extended cloud phase is fog, water or supercooled and $T_c \leq 231$ K, it is re-set to cirrus or opaque ice (if cloud optical thickness has been retrieved and is larger than 3). If the extended cloud phase is opaque ice, cirrus, overlap or overshooting, and $T_c \geq 265$ K, it is re-set to supercooled (if $T_c < 273$ K) or water (if $T_c \geq 273$ K).

Finally, the extended phase is reduced to a binary cloud-top phase product, by setting the categories fog, water and supercooled to liquid and the categories opaque ice, cirrus, overlap and overshooting to ice. While during nighttime this is the final retrieved phase, during daytime this phase is the starting point of the optical properties retrieval process, through which it can still be modified if it turns out to be incompatible with the observed VIS-NIR reflectance pair. This is further explained in Section 4.3.2.

4.3.1.1 AVHRR

The cloud phase retrieval is based on a number of threshold tests using AVHRR channels 3a, 3b, 4 and 5 or corresponding channels from VIIRS, MODIS or MERSI-2 (see Section 4.5.1). The algorithm is run for cloudy pixels and yields one of the following extended cloud phase categories: fog, liquid, supercooled, opaque ice, cirrus, and overlap (ice above liquid). Separate retrieval schemes are applied during daytime and nighttime. An extensive motivation for and description of the several spectral tests is given in Pavolonis and Heidinger (2004) and Pavolonis et al. (2005). Here, we provide a complete overview of the spectral tests and the order in which they are performed. Values of the thresholds are given in ANNEX B.

The algorithm contains a number of tests using the 3.8 μm reflectance ($R_{3.8}$) during daytime or emissivity ($\varepsilon_{3.8}$) during night time. These are estimated from the 3.8 and 11 μm radiances alone. For the 3.8 μm radiance $L_{3.8}$ we have:

$$L_{3.8} = R_{3.8} \frac{\mu_0 F_{0,3.8}}{\pi} + \varepsilon_{3.8} L_{bb,3.8} \quad (12)$$

where $L_{bb,3.8}$ is the black-body radiance at 3.8 μm . Assuming an 11 μm emissivity of one (i.e. opaque clouds) yields:

$$L_{bb,3.8} = B_{3.8}(T_{bb}) = B_{3.8}(T_{11}) \quad (13)$$

where T_{11} is the brightness temperature at 11 μm and T_{bb} is the blackbody temperature. Assuming then also zero 3.8 μm transmissivity (again: opaque clouds), we have:

$$\varepsilon_{3.8} = 1 - R_{3.8} \quad (14)$$

<i>EUMETSAT Satellite Application Facility to NoWCASTing & Very Short Range Forecasting</i>	Algorithm Theoretical Basis Document for Cloud Micro Physics of the NWC/PPS	Code: NWC/CDOP3/PPS/SMHI/SCI/ATBD/CMIC Issue: 3.1.0 Date: 01 September 2022 File: NWC-CDOP3-PPS-SMHI-SCI-ATBD-CMIC_v3_1_0 Page: 29/49
---	---	---

Inserting Eqs. (13) and (14) in (12) yields:

$$R_{3.8} = \frac{L_{3.8} - B_{3.8}(T_{11})}{\frac{\mu_0 F_{0,3.8}}{\pi} - B_{3.8}(T_{11})} \quad (15)$$

and the emissivity during night time is:

$$\epsilon_{3.8} = \frac{L_{3.8}}{B_{3.8}(T_{11})} \quad (16)$$

As stated above, these relations assume opaque clouds. Indeed, the NIR reflectance tests are less reliable for thin clouds (see Pavolonis et al. 2005, Sect. 6). The algorithm starts with an initial cloud phase assignment based on T_{11} :

- $T_{11} \leq 253.16$ K \rightarrow opaque ice
- 253.16 K $< T_{11} \leq 273.16$ K \rightarrow supercooled
- $T_{11} > 273.16$ K \rightarrow water

The *daytime* ($\theta_0 < 88^\circ$) algorithm then proceeds with the following tests, in which R_{NIR} is either $R_{1.6}$ or $R_{3.8}$, depending on the available channel.

D1: First NIR reflectance test

Clouds classified as supercooled, with $T_{11} < 263.16$ K, and $R_{\text{NIR}} \leq \text{NIR_PHASE_THRES}$, are re-set to opaque ice. Here, NIR_PHASE_THRES depends on the NIR channel used and the surface type (see Appendix).

D2: Second NIR reflectance test ('inverse' of d1)

Clouds classified as opaque ice, with $T_{11} > 233.16$ K, and $R_{\text{NIR}} > \text{NIR_PHASE_THRES}$, are re-set to supercooled.

D3: Cloud overlap test

Clouds with a $T_{11} - T_{12}$ difference larger than $\text{BTD1112_DOVERLAP_THRES}$, with 210 K $< T_{11} < 270$ K, with $R_{\text{NIR}} > \text{NIR_OVER_THRES}$, and not over desert, are set to overlap. Here, $\text{BTD1112_DOVERLAP_THRES}$ depends on $R_{0.6}$, as well as on θ and θ_0 , and NIR_OVER_THRES depends on the NIR channel used and the surface type (see Appendix).

D4: Cirrus test

Clouds with a $T_{11} - T_{12}$ difference larger than $\text{BTD1112_CIRRUS_THRES}$, with $T_{11} < 295$ K, with $R_{\text{NIR}} < \text{NIR_CIRRUS_THRES}$, and not classified as overlap, are set to cirrus. The R_{NIR} criterion is not applied if $\theta_0 > 70^\circ$, but the cirrus is assigned a 'low quality' in this case. $\text{BTD1112_CIRRUS_THRES}$ depends on T_{11} and θ , and NIR_CIRRUS_THRES depends on the NIR channel used and the surface type (see Appendix).

D5: Fog test

Only performed if ch3b is available: if $R_{3.8} \geq 0.25$, $R_{3.8}/R_{0.6} < 0.6$, $T_{11} > 240$ K, and the surface is not desert, the cloud is classified as fog.

The *nighttime* ($\theta_0 \geq 88^\circ$) algorithm proceeds with the following tests.

N1: First 3.8 μm emissivity test

Clouds classified as supercooled, with $T_{11} < 263.16$ K, and $\epsilon_{3.8} \geq \text{EMS38_PHASE_THRES}$, are re-set to opaque_ice. Here, EMS38_PHASE_THRES depends on T_{11} .

N2: Second 3.8 μm emissivity test ('inverse' of n1)

<i>EUMETSAT Satellite Application Facility to NoWCASTing & Very Short Range Forecasting</i>	Algorithm Theoretical Basis Document for Cloud Micro Physics of the NWC/PPS	Code: NWC/CDOP3/PPS/SMHI/SCI/ATBD/CMIC Issue: 3.1.0 Date: 01 September 2022 File: NWC-CDOP3-PPS-SMHI-SCI-ATBD-CMIC_v3_1_0 Page: 30/49
---	---	---

Clouds classified as opaque ice, with $T_{11} > 233.16$ K, and $\varepsilon_{3.8} < \text{EMS38_PHASE_THRES}$, are re-set to supercooled.

N3: Cloud overlap test

Clouds with $\text{BTD1112_NOVERLAP_THRES_L} < T_{11} - T_{12} < \text{BTD1112_NOVERLAP_THRES_H}$, $210 \text{ K} < T_{11} < 283 \text{ K}$, and $\text{EMS38_NOVERLAP_THRES_L} < \varepsilon_{3.8} < \text{EMS38_NOVERLAP_THRES_H}$ are set to overlap. Here, the thresholds vary between tropical and extratropical areas, and between surface types (see Appendix).

N4a: First cirrus test

Clouds with $T_{11} - T_{12} > \text{BTD1112_CIRRUS_THRES}$ and $\varepsilon_{3.8} > 1.3$, and not classified as overlap, are set to cirrus.

N4b: Second cirrus test

Clouds with $T_{11} < 300 \text{ K}$ and $\varepsilon_{3.8} > 1.1$, and not classified as overlap or opaque ice, are set to cirrus.

N5: Fog test

If $\varepsilon_{3.8} \leq 0.9$, $T_{11} > 240 \text{ K}$, $\theta_0 \geq 90^\circ$ and the surface is not desert, the cloud is classified as fog.

Finally, after the day or night portion of the algorithm, a spatial filter on cirrus and overlap pixels is applied, in which the minimum of T_{11} and the mean of $\varepsilon_{3.8}$ in a 7x7 pixels box around the pixel of interest are considered.

S1: Spatial test to re-set cirrus to liquid

If a pixel is classified as cirrus with a low quality, and either the pixels in the box have $\text{MIN}(T_{11}) > 295 - 12(1-\theta)$ or $\text{MEAN}(\varepsilon_{3.8}) < 1.2$, then the pixel is re-set to supercooled (if $T_{11} \leq 273.16 \text{ K}$) or water (if $T_{11} > 273.16 \text{ K}$).

s2: Spatial test to re-set overlap to liquid

If a pixel is classified as overlap, $\theta_0 > 90^\circ$, and the pixels in the box have $\text{MIN}(T_{11}) > 273 - 12(1-\theta)$, then the pixel is re-set to supercooled (if $T_{11} \leq 273.16 \text{ K}$) or water (if $T_{11} > 273.16 \text{ K}$).

Note that on the AVHRR/1 series T_{12} is not measured. In this case, the corresponding tests (d3, d4, n3 and n4a) are skipped, which mainly affects the identification of cirrus and overlap types.

4.3.1.2 **METimage**

For day-1 METimage will use the AVHRR heritage channels and the same algorithm as used by AVHRR. However some of the channels available on METimage in theory make an improved cloud phase product possible. The usage of channels $3.8 \mu\text{m}$ (solar-thermal IR), $6.7 \mu\text{m}$ (water vapour), $8.5 \mu\text{m}$ (window), and $13 \mu\text{m}$ (CO_2) and $1.38 \mu\text{m}$ could improve cloud phase detection. The channel $2.2 \mu\text{m}$ will be added in the day-1 release, though configurable. For day-2 the algorithm choice for cloud phase will be reconsidered. The new algorithm (TBD03) should better exploit the METimage capabilities of 20 channels, improve detection skill while still meeting the timeliness requirements.

4.3.2. Cloud optical properties

For the cloud optical property retrieval, the observed VIS and NIR reflectances are compared with the simulated reflectances in the LUT. For the VIS reflectance the $0.6\text{-}\mu\text{m}$ channel is normally

<i>EUMETSAT Satellite Application Facility to NoWCasting & Very Short Range Forecasting</i>	Algorithm Theoretical Basis Document for Cloud Micro Physics of the NWC/PPS	Code: NWC/CDOP3/PPS/SMHI/SCI/ATBD/CMIC Issue: 3.1.0 Date: 01 September 2022 File: NWC-CDOP3-PPS-SMHI-SCI-ATBD-CMIC_v3_1_0 Page: 31/49
---	---	---

used. More modern imagers, in particular VIIRS and METImage as well as MODIS, carry a channel near 1.24 μm . This channel offers much improved capability for the retrieval of cloud optical thickness over snow- or ice-covered surfaces. In the operational MODIS processing (MOD06) it has been used for these conditions for a long time, and we intend to follow that approach as well. Note that 1.24 μm is obviously not in the VIS wavelength range, but it can be used as the ‘first’ channel in the Nakajima-King retrieval, instead of the VIS 0.6- μm channel.

For the NIR reflectance, several choices are possible. From the AVHRR heritage the 1.6- and 3.8- μm channels are used, and these have been extensively discussed in the current ATBD. However, on VIIRS and METImage, a channel near 2.25 μm is available, offering excellent opportunities for the retrieval of effective radius, which will be exploited.

In case the 3.8- μm channel is used as NIR channel, the observed radiance is expressed as a reflectance rather than a brightness temperature:

$$R_{3.8} = \frac{\pi L_{3.8}}{\mu_0 F_{0,3.8}} \quad (17)$$

which is then compared with the sum of simulated solar reflectance (from the DAK LUT) and thermal emission cast as a reflectance (from Eq. (10)). The cloud optical thickness and particle size are retrieved in an iterative manner for cloudy pixels during daytime ($\theta_0 < 84^\circ$). During the iteration the retrieval of τ at the 0.6- μm channel is used to update the retrieval of r_e at the 1.6/2.2/3.8- μm channel, and vice versa. This iteration process continues until the retrieved cloud optical properties converge to stable values. The interpolation between cloud optical properties in the LUTs is done with cubic splines in τ for the smaller half of the τ -axis and in $\log(\tau)$ for the larger half of the τ -axis, while cubic splines in $\log(r_e)$ are applied for the whole r_e -axis.

If the observed reflectance pair is located outside the LUT space, the nearest solution at the border of the LUT space is reported. This is achieved by limiting τ and of r_e to their extreme values in the LUT axes in the iterative process described above. However, if the assigned phase is liquid and the observed reflectance pair lies ‘below’ (as in Figure 4) the liquid cloud LUT space, and if in addition the cloud top is not too warm (i.e. $T_c < 265$ K), the phase is reset to ice followed by a new $\tau - r_e$ retrieval attempt for an ice cloud. Similarly, if the assigned phase is ice and the observed reflectance pair lies ‘above’ the ice cloud LUT space, and if in addition the cloud top is not too cold (i.e. $T_c > 231$ K), the phase is reset to liquid followed by a new $\tau - r_e$ retrieval attempt for a liquid cloud. Via this mechanism the phase can be changed compared to what was described in Section 4.3.1, reflecting an important role of the NIR channel in the phase retrieval during daytime. If a phase switch occurs, the extended phase is adjusted accordingly: in the case of a switch from liquid to ice, the extended phase is re-set to cirrus (if $\tau \leq 3$) or opaque (if $\tau > 3$); in the case of a switch from ice to liquid, the extended phase is re-set to water.

4.4. ERROR BUDGET ESTIMATES

The retrieval of cloud optical thickness and cloud particle effective radius from 2-channel backscattered solar radiation is a simple but heavily underconstrained problem. As a result, many uncertainties are associated to this retrieval problem (see Stephens and Kummerow (2007) for a review). In this section we first discuss a number of error sources which are not explicitly taken into account, and then explain the propagation of uncertainties that are taken into account, including in the observations and some of the ancillary data. Finally, a brief characterization of the resulting uncertainty estimates is given, focusing on the 0.6-1.6 and 0.6-3.8 μm channel retrievals.

<i>EUMETSAT Satellite Application Facility to NoWCasting & Very Short Range Forecasting</i>	Algorithm Theoretical Basis Document for Cloud Micro Physics of the NWC/PPS	Code: NWC/CDOP3/PPS/SMHI/SCI/ATBD/CMIC Issue: 3.1.0 Date: 01 September 2022 File: NWC-CDOP3-PPS-SMHI-SCI-ATBD-CMIC_v3_1_0 Page: 32/49
---	---	---

The first part of the CMIC retrieval is the determination of cloud phase. Similar to most existing cloud phase retrieval schemes (e.g., for MODIS: Platnick et al., 2017) no uncertainty estimate is derived for the phase retrieval. In [RD.3], cloud phase is validated with CALIOP observations, and the fraction of wrong phase retrievals is stratified according to CTTH errors and cloud type. It turns out that phase misclassifications occur most frequently when the CTTH error, both the actual value and its estimate, is large and for thin cirrus and mid-level cloud types. If the CTTH error is smaller than 50 hPa, only 7-9% of the phase retrievals is wrong, in comparison to 14-19% for all pixels. Phase misclassifications become even more infrequent if homogeneous scenes with known (and correct) surface type are selected. From this analysis it is concluded that the bulk of the phase uncertainty comes from CTTH and other input errors as well as scene inhomogeneities and differences between field of view from the passive imager compared to the reference observations, while algorithmic errors, including errors in the underlying RTM simulations, contribute much less. Flagging of potentially uncertain phase classifications can be done on the basis of the CTTH error estimate, and in addition the *cmic_quality* flag (Table 17).

For well-described cloudy cases, errors in forward radiative transfer modelling were analysed by Roebeling et al. (2005), comparing three RTMs that use different methods to solve the equation of radiative transfer to a Monte Carlo model (Macke et al., 1999). Apart from DAK, used for the radiative transfer calculations underlying CMIC/CPP, the Spherical Harmonics Discrete Ordinate Method (SHDOM: Evans 1998) and MODTRAN 4v2r0 (Berk et al., 2000), in which the multiple scattering calculations are based on the Discrete Ordinate (DISORT) method (Stamnes et al. 1988), were tested. In this analysis, DAK and SHDOM were found to agree rather closely in terms of top-of-atmosphere radiances over a range of cloudy cases, with a standard deviation of about 2% compared to the Monte Carlo model, but also an unexplained bias of about 3%. MODTRAN showed somewhat larger deviations, which were probably related to the preliminary status (beta release) of the version that was used. Differences between the RTMs depend on cloud properties as well as solar and viewing angles. Overall it was concluded that DAK RTM errors are small, and since there furthermore is no true reference to quantify errors against, it was decided to neglect the uncertainties related to radiative transfer for the estimation of retrieval uncertainties.

The comparisons described before were performed for idealized, plane-parallel, vertically homogenous, single-layer, single-phase clouds. These assumptions are usually violated, giving rises to potentially very large retrieval errors. They are discussed in more detail in Section 5, but are not taken into account in the uncertainty estimates. It should further be noted that since no uncertainty is associated to the cloud phase retrieval, its impact on the cloud optical and microphysical properties uncertainty is also neglected. Now we turn our attention to the error sources that are taken into account and how uncertainty estimates are derived from them.

The following relation, which is the same as used in optimal estimation but in absence of *a priori* information (Rodgers, 2000), is applied to obtain the covariance matrix of retrieval uncertainties \mathbf{S}_r :

$$\mathbf{S}_r = \mathbf{K}^{-1} \mathbf{S}_y (\mathbf{K}^{-1})^T + \sum_i (\mathbf{K}^{-1} \mathbf{K}_{b_i}) \mathbf{S}_{b_i} (\mathbf{K}^{-1} \mathbf{K}_{b_i})^T \quad (18)$$

The first term describes the propagation of observation errors, where \mathbf{S}_y (2x2, diagonal) is the observation error covariance matrix. \mathbf{K} is the (2x2) Jacobian matrix containing the partial derivatives of TOA reflectance in each channel with respect to the retrieval variables τ and r_e . It is approximated from the gradients in the LUT. The second term describes the propagation of model errors. It is a summation over the different model / ancillary data error sources (e.g., water vapour path), where \mathbf{S}_{b_i} are the corresponding error covariance matrices. In our case, all error sources are assumed to be independent, and all \mathbf{S}_{b_i} are 1x1 matrices. The 2x1 matrices \mathbf{K}_{b_i} contain the partial derivatives of the simulated reflectance in each channel with respect to the particular error source.

Only the (square root of the) diagonal elements of \mathbf{S}_r , denoted σ_τ and σ_{r_e} , are reported in the CMIC output.

The LWP/IWP (here combinedly denoted by CWP), CDNC and CGT uncertainties can be calculated by propagating the uncertainties in COT and CRE in Eqs. (19) – (21):

$$\frac{\sigma_W}{CWP} = \frac{\sigma_\tau}{\tau} + \frac{\sigma_{r_e}}{r_e} \quad (19)$$

$$\frac{\sigma_{N_d}}{N_d} = 0.5 \frac{\sigma_\tau}{\tau} + 2.5 \frac{\sigma_{r_e}}{r_e} \quad (20)$$

$$\frac{\sigma_{H_g}}{H_g} = 0.5 \frac{\sigma_\tau}{\tau} + 0.5 \frac{\sigma_{r_e}}{r_e} \quad (21)$$

An overview of the error sources considered is given in Table 9. Specification of the uncertainties in the driving parameters approximately follows Platnick et al. (2017). For the reflectances, the bulk of systematic errors is thought to have been removed by careful calibration (e.g., Heidinger et al., 2010). Here, the uncertainty is assumed to be 3% for all channels. The impact of uncertainties in several ancillary datasets is also quantified. Surface albedo is assumed to have a 15% (relative) uncertainty in all channels. As discussed in Section 4.2, atmospheric absorption is influenced by the total ozone column, water vapour path and cloud top height, which are assigned relative uncertainties of 15%, 10% and 20%, respectively. Thermal emission, relevant in the 3.8- μm channel, depends mainly on surface temperature and cloud top temperature, while the parameters determining atmospheric absorption (except ozone, which does not play a role at 3.8 μm) also contribute. The surface temperature uncertainty is assumed to be 1.5 K. The cloud top temperature uncertainty is related to the cloud top height uncertainty on the basis of a lapse rate of 6.5 K km^{-1} . The cloud top height and temperature uncertainties are specified in a generic way based on results of validation with active instruments (Häkansson et al., 2018), rather than adopting the uncertainties associated with the pixel-level retrieval products used as input.

Table 9: Error sources taken into account for CMIC retrieval uncertainty estimates.

Error source	Parameter	Specification
Observations	Reflectance VIS and NIR	3% (relative)
Land/ocean reflectance	Surface albedo VIS and NIR	15% (relative)
Atmospheric absorption	Total column ozone	15%
	Water vapour path	10%
	Cloud top height	20%

Error source	Parameter	Specification
Thermal emission (3.8 μm)	Surface temperature	1.5 K
	Cloud top temperature	6.5 ΔCTH (K)

An indication of the magnitude of the estimated uncertainties and the contribution of the different error sources is given in Table 10. Note that these numbers were derived from MSG-SEVIRI retrievals. They should be very similar for AVHRR, although small differences will be caused by the different spectral response functions of the respective channels. The main error source for the COT retrieval is the visible reflectance. For CRE, the picture is more diverse. In case of the 0.6–1.6 μm channel combination, the NIR reflectance plays the main role. However, the VIS reflectance is also important, contributing about as much to the total uncertainty as the NIR reflectance, at least for liquid water clouds. This can be explained by the non-orthogonality of the LUT, especially for thin clouds. In case of the 0.6–3.8 μm channel combination, the correction for thermal emission and atmospheric absorption, for which uncertainties are driven mainly by the cloud top temperature and height, respectively, contribute most to the total CRE uncertainty.

Table 10: Relative uncertainties (in %) in COT and CRE retrievals as a total and separated by error source. The numbers reflect the median uncertainties from a full disk worth of SEVIRI retrievals (7 March 2017, 14:00 UTC). Pixels for which the observations were outside the look-up table or the visible surface albedo was larger than 0.6 were excluded. Results are shown separately for the 0.6–1.6 μm and the 0.6–3.8 μm retrievals as well as for liquid and ice clouds. Rows with a grey background contain the main error sources, some of which have been further separated as shown in the rows with a white background. The total uncertainty and the individual error source contributing most to the total uncertainty are indicated in bold face.

Error source	0.6–1.6 μm				0.6–3.8 μm			
	COT		CRE		COT		CRE	
	liquid	ice	liquid	ice	liquid	ice	liquid	ice
VIS reflectance	9.7	8.2	14.0	3.6	7.6	8.4	0.5	3.3
NIR reflectance	2.5	0.3	15.0	8.3	1.4	0.2	6.7	4.3
VIS+NIR refl.	10.1	8.3	21.0	9.6	7.9	8.4	6.7	6.0
VIS surface albedo	2.4	1.1	3.9	0.6	1.5	1.0	0.1	0.5
NIR surface albedo	0.7	0.2	4.5	2.2	0.2	0.2	0.2	0.1
VIS+NIR surf. Albedo	2.6	1.1	6.6	2.6	1.5	1.0	0.3	0.6
Absorption ozone	3.2	2.9	4.3	1.1	2.8	3.0	0.2	1.0
Absorption H_c	0.5	0.4	1.9	1.1	1.6	0.4	9.3	4.8
Absorption WVP	0.2	0.2	0.1	0.0	0.4	0.2	2.0	0.5
Absorption non-ozone	0.5	0.4	1.9	1.1	1.6	0.4	9.5	5.0
Emissivity T_s					0.3	0.2	1.3	1.7

Emissivity T_c					1.6	0.3	8.3	9.2
Emissivity total					1.8	0.3	9.9	13.8
Total	12.8	10.1	24.7	11.6	9.9	10.1	16.2	18.1

The numbers in Table 10 provide only a coarse indication of the uncertainty contributions. Results depend considerably on the surface type and atmospheric composition, and most importantly on the cloud properties themselves. The latter is illustrated in Figure 5 for the 0.6–1.6 μm retrieval. The relative COT uncertainty minimizes around COT=5, while it does not depend much on CRE. As noticed before, the main error source is the VIS reflectance. However, for thin clouds, surface albedo becomes an equally important error source. The relative CRE uncertainty decreases with COT, and reaches values over 50% for thin clouds. For most of the COT range, the CRE uncertainty is dominated by the NIR reflectance, while for thin clouds surface albedo (both VIS and NIR) becomes an even more important error source. Broadly, the relative CRE uncertainty also decreases with CRE. Figure 6 shows similar plots as Figure 5, but for the 0.6–3.8 μm channel combination. The results are comparable to each other in the case of COT, but for CRE the major contribution of in particular thermal emission to the uncertainty is evident. The difficulty to retrieve CRE for thin clouds is less severe when using the 3.8 μm channel, as is demonstrated by the much lower CRE uncertainties in the small-COT range. However, toward large effective radii, the CRE uncertainty becomes very large and exceeds 50%. The reason is that the reflectance of clouds with larger ice particles becomes very low (see Figure 4), and lines of different CRE are almost on top of each other.

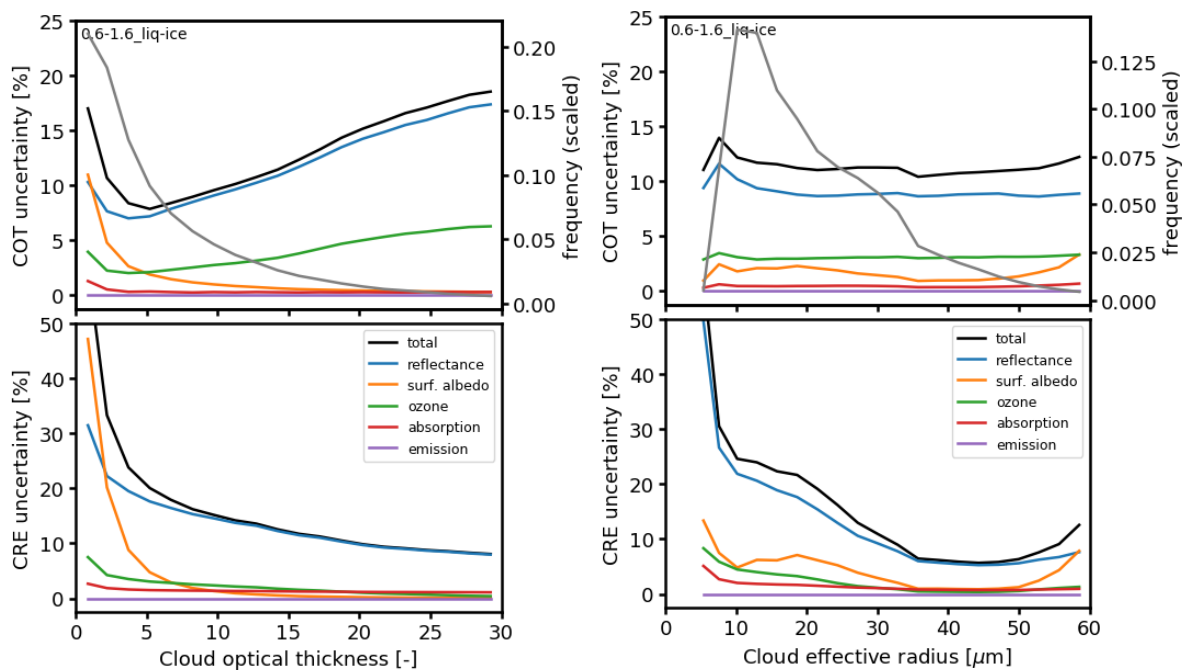


Figure 5: Dependence of COT and CRE uncertainties on COT and CRE of both liquid and ice clouds for the 0.6–1.6 micron retrieval. Uncertainties due to different error sources are shown separately. COT and CRE histograms are indicated by the grey lines.

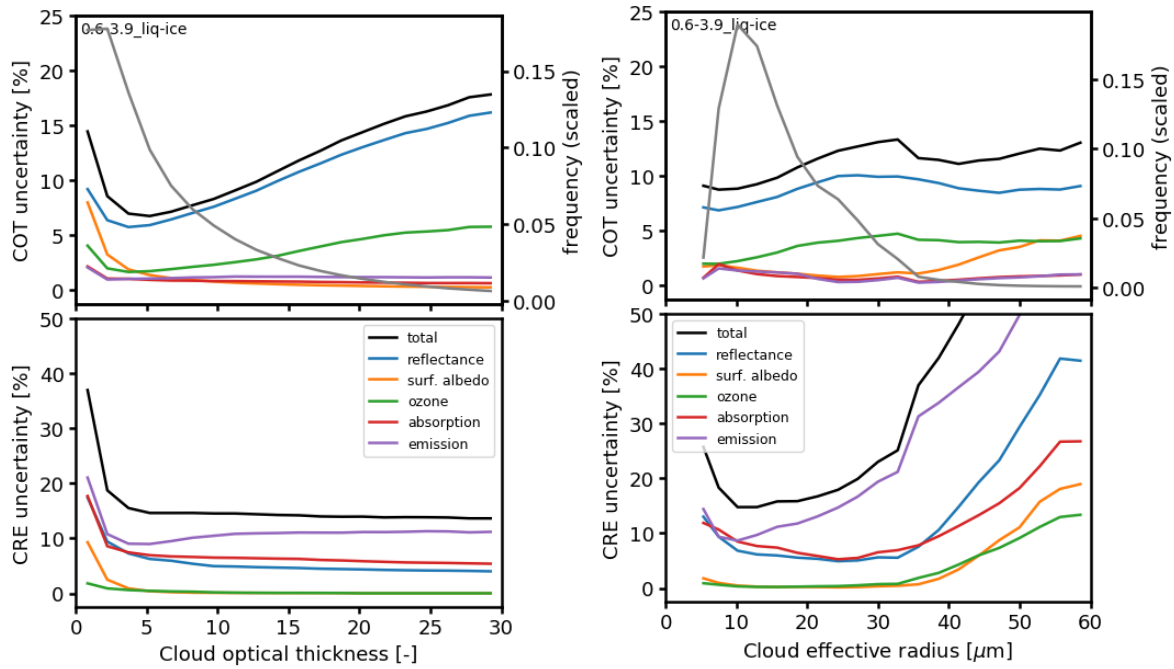


Figure 6: As Figure 5, but for the 0.6–3.8 micron retrieval.

Finally, the retrieval uncertainties are displayed against two ancillary parameters in Figure 7. This shows that the COT uncertainty increases considerably with solar zenith angle, while CRE shows a limited sensitivity. It should be noted that, since this analysis is based on SEVIRI observations, the solar zenith angle is correlated with the satellite zenith angle, so tendencies may also be related to that variable. The right panel in Figure 7 illustrates the enormous effect of the surface albedo: the COT uncertainty increases sharply for brighter surfaces and reaches the maximum reported value of 100% around a VIS surface albedo of 60%. The reason for these high uncertainties is that clouds can hardly be distinguished from such clear backgrounds.

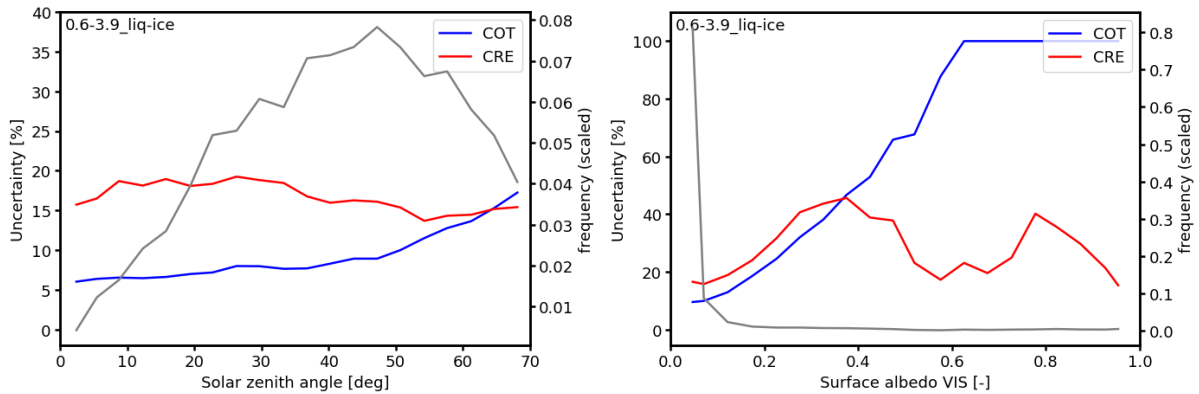


Figure 7: COT and CRE uncertainties as a function of solar zenith angle (left) and VIS surface albedo (right). COT and CRE histograms are indicated by the grey lines.

4.5. PRACTICAL APPLICATION

This section provides details on the satellite instruments (AVHRR, METimage, VIIRS, MODIS and MERSI-2) and other input data used by the CMIC algorithm.

4.5.1. Satellite instruments

Both EUMETSAT and NOAA have previously launched a series of polar orbiting satellites that carry the AVHRR instrument. The latest series of AVHRR passive imager (AVHRR/3) operates six channels at wavelengths between 0.5 and 12.0 μm . Table 11 summarizes the AVHRR channels used by CMIC. Due to fundamental constraints, the near-infrared 1.6 μm and 3.8 μm channels are time-shared. On NOAA-16 (during the first two years of its life), NOAA-17, and METOP the 1.6- μm channel has been operated during the daylight part of the orbit, while the 3.8- μm channel was operated during night. All other NOAA satellites have only transmitted data from the 3.8- μm channel. Moreover, the earlier AVHRR/1 and AVHRR/2 series carried only 4 and 5 channels, respectively, as indicated in Table 11. The spatial resolution of all channels at nadir is around $1 \times 1 \text{ km}^2$, but this is degraded to $5 \times 4 \text{ km}^2$ for GAC-AVHRR.

Table 11: AVHRR channels used by CMIC

Channel	Central wavelength (μm)	Nominal spectral band (μm)
1	0.63	0.58 – 0.68
3a ^{a) b)}	1.61	1.58 – 1.64
3b ^{a)}	3.74	3.55 – 3.93
4	10.8	10.30 – 11.30
5 ^{c)}	12.0	11.50 – 12.50

^{a)} Only one NIR channel at the same time can be transmitted to the ground.

^{b)} Not present on the AVHRR/1 and AVHRR/2 series

^{c)} Not present on the AVHRR/1 series

NOAA has also launched the polar satellite NPP, which will be followed by a series of JPSS satellites. All of them carry the sensor VIIRS. Table 12 summarizes the VIIRS channels used by CMIC. The spatial resolution of these channels is $750 \times 750 \text{ m}^2$ at nadir. CMIC can be run with VIIRS data from either M10 or M12 as absorbing channel. The channels that are not AVHRR-heritage (i.e. M8, M9 and M11) will not be used in PPS v2021. For PPS vEPSSG day1 channel M11 will be included, as optional. The usage of other non AVHRR-heritage channels is (TBD03) for PPS vEPSSG day2.

Table 12: VIIRS channels used by CMIC.

Channel	Central wavelength (μm)	Nominal spectral band (μm)
M5	0.672	0.662 – 0.682
M8	1.24	1.23 – 1.25
M9	1.38	1.37 – 1.39
M10	1.61	1.58 – 1.64
M11	2.25	2.225 – 2.275
M12	3.70	3.61 – 3.79
M15	10.76	10.26 – 11.26
M16	12.01	11.54 – 12.49

CMIC can also be run in high resolution, using a combination of VIIRS data from the I-band and M-band channels. Table 13 describes which channels are needed (and M11 which is optional).

The spatial resolution for the I-band channels is $375 \times 375 \text{ m}^2$ at nadir. The M-band channels are interpolated to that resolution, before using them in PPS.

Table 13: VIIRS channels used by CMIC, for running in high resolution.

<i>Channel</i>	<i>Central wavelength (μm)</i>	<i>Nominal spectral band (μm)</i>
I1	0.64	0.60-0.68
I3	1.61	1.58-1.64
I4	3.74	3.55-3.93
M11	2.25	2.225 – 2.275
M15	10.76	10.26 – 11.26
M16	12.01	11.54 – 12.49

The MODIS instrument on board the EOS-Terra and EOS-Aqua platforms has 36 channels. Table 14 summarizes the channels used by CMIC. The spatial resolution of these channels varies from $250 \times 250 \text{ m}^2$ to $1 \times 1 \text{ km}^2$.

Table 14: MODIS channels used by CMIC.

<i>Channel</i>	<i>Central wavelength (μm)</i>	<i>Nominal spectral band (μm)</i>
1	0.645	0.620 – 0.670
6	1.640	1.628 – 1.652
20	3.750	3.660 – 3.840
31	11.03	10.78 – 11.28
32	12.02	11.77 – 12.27

The MERSI-2 instrument will be launched on the FY-3D and FY-3E satellites. It has 25 channels at a spatial resolution varying between $250 \times 250 \text{ m}^2$ and $1 \times 1 \text{ km}^2$. Table 15 summarizes the channels used by CMIC.

Table 15: MERSI-2 channels used by CMIC.

<i>Channel</i>	<i>Central wavelength (μm)</i>	<i>Nominal spectral band (μm)</i>
7	0.650	0.625 – 0.675
18	1.640	1.615 – 1.665
20	3.80	3.71 – 3.89
24	10.8	10.3 – 11.3
25	12.0	11.5 – 12.5

The METImage instrument will be launched on the Metop-SG-A satellites. It has 20 channels at a spatial resolution of $500 \times 500 \text{ m}^2$ at sub-satellite point. Table 16 summarizes the channels used by CMIC, though not all use used yet in PPS vEPSSG (TBD03).

Table 16: METImage channels used by CMIC.

<i>Channel</i>	<i>Central wavelength (μm)</i>	<i>Nominal spectral band (μm)</i>
VII-12	0.668	0.658 – 0.678
VII-22	1.24	1.23 – 1.25
VII-23	1.38	1.36 – 1.40
VII-24	1.63	1.62 – 1.64
VII-25	2.25	2.225 – 2.275
VII-26	3.74	3.65 – 3.83
VII-37	10.69	10.44 – 10.94
VII-39	12.02	11.77 – 12.27

4.5.2. Input data

In this section, the required input data for the algorithms are described

4.5.2.1 *Radiances*

Radiances from 0.6- μm , 1.6- μm or 2.2- μm or 3.8- μm , 11- μm , and 12- μm channels are the basic input.

Radiance for 2.2- μm can also be used, if available. It is also configurable not to use it.

4.5.2.2 *Solar and satellite angles*

The solar zenith angle θ_0 , the satellite viewing zenith angle θ , and the relative sun-satellite azimuth angle ϕ are required. These angles are calculated by the NWC-SAF software and provided as input to CMIC.

4.5.2.3 *Cloud mask*

A cloud mask is needed to decide for which pixels a cloud micro physics retrieval will be attempted. As default, the cloud mask (Cma) of the NWC-SAF is used for this purpose (see [RD.5]). The CMIC retrievals are run for pixels classified as *cloud contaminated* or *cloud filled*.

An alternative input (configurable) is the Cloud Probability (CMA-prob) product instead. The CMIC retrievals are run for pixels with a cloud probability of 50% or more. (Configurable via `pps_product_config.yaml/cmaprob_cloud_threshold` (PPSv2021) or environment variable `SM_CMAPROB_CLOUD_THRESHOLD` (PPSv2018).)

4.5.2.4 *Cloud top height and temperature*

CMIC uses the cloud top temperature and height, which are taken from the CTTH product from NWC-SAF ([RD.6]). It can also manage without the CTTH-product, or with only one of cloud top temperature or height available.

<i>EUMETSAT Satellite Application Facility to NoWCASTing & Very Short Range Forecasting</i>	Algorithm Theoretical Basis Document for Cloud Micro Physics of the NWC/PPS	Code: NWC/CDOP3/PPS/SMHI/SCI/ATBD/CMIC Issue: 3.1.0 Date: 01 September 2022 File: NWC-CDOP3-PPS-SMHI-SCI-ATBD-CMIC_v3_1_0 Page: 40/49
---	---	---

4.5.2.5 *Surface albedo*

A spatially complete (gap-filled) global land surface albedo dataset, in both the VIS and NIR spectral channels used in CMIC, is required for the cloud retrievals. A corresponding climatology was created based on the gap-filled snow-free MODIS Collection 6 level 3 white-sky albedo dataset (MCD43GF) for the required channels (Sun et al. 2017). These data are available globally on a daily basis and on a ~ 1000 m latitude-longitude grid, and span the period 2000-2017. Here, data from the period 2003-2017 were used, which are based on both Terra and Aqua full-year retrievals. The climatology was computed on a daily basis and on a $0.05^\circ \times 0.05^\circ$ latitude-longitude grid. To this end, the original MCD43GF albedo data were averaged on a 6×6 grid cells basis, to match the desired resolution. Corresponding quality indices (0-7, 0 being the best quality) were also averaged, and the reciprocal of their average was used as weight of the resulting 0.05° grid cell albedo in the temporal averaging (to avoid divisions by zero, the value 1 was first added to all quality indices; thus, best quality values have weight 1, and worst quality values have weight 0.125). The climatological value for a grid cell and a specific day in the year was then computed as the weighted average of values from the 15 available years. Over coastal areas, an additional step was taken: after calculating the land albedo as before, the 0.05° grid cell albedo was calculated as $\alpha_s = \alpha_{s,land}f_{land} + \alpha_{s,ocean}(1 - f_{land})$, where f_{land} , the fraction of land, was calculated as the fraction of $6 \times 6 = 36$ MCD43GF grid cells available.

For the white-sky surface albedo over ocean, constant values are prescribed based on Jin et al. (2011). These values, 4.8%, 4.4%, 4.1%, and 4.9%, for the 0.6-, 1.6-, 2.2- and 3.8- μm channels, respectively, were calculated for a wind speed of 10 m s^{-1} . Variations with wind speed are less than 0.4% up to 15 m s^{-1} . At higher wind speeds, whitecap foam causes a somewhat larger increase in albedo, but this is neglected here.

4.5.2.6 *Surface emissivity*

For the 3.8- μm retrieval, a climatology compiled from four years of the MODIS-based surface emissivity database by Seemann et al. (2008) is used over land. Thus both the surface albedo and emissivity inputs are consistently based on MODIS observations. Over ocean the surface emissivity is set to 1 minus the surface albedo mentioned in the previous subsection, i.e. 95.1%.

4.5.2.7 *Numerical Weather Prediction (NWP) model fields*

The following NWP model fields are required:

- Vertical profiles of temperature, pressure and humidity; 2-meter values of temperature, wind, and humidity; skin temperature; surface pressure. These are needed for the clear-sky and overcast radiance calculations (TBD03). The skin temperature is also needed for the 3.8- μm CMIC retrieval.
- Water vapour path. For the atmospheric correction the water vapour path is needed. As a back-up it is possible to use a monthly-mean climatology based on ERA-Interim data.
- Snow depth and snow albedo. These are used for the cloud phase determination and to correct the MODIS albedo in case of snow on the ground. The snow depth d_{snow} , in m water equivalent, is converted to a snow cover fraction f_{snow} according to $f_{snow} = \text{MIN}(d_{snow}/0.1, 1)$. The snow cover fraction is then used as a weight between the NWP snow albedo $\alpha_{s,snow}$, converted to the specific channels using fixed conversion factors, and the snow-free MODIS surface albedo: i.e. $\alpha_s = \alpha_{s,snow}f_{snow} + \alpha_{s,MODIS}(1 - f_{snow})$. The snow parameters are not mandatory input, in the sense that the

<i>EUMETSAT Satellite Application Facility to NoWCasting & Very Short Range Forecasting</i>	Algorithm Theoretical Basis Document for Cloud Micro Physics of the NWC/PPS	Code: NWC/CDOP3/PPS/SMHI/SCI/ATBD/CMIC Issue: 3.1.0 Date: 01 September 2022 File: NWC-CDOP3-PPS-SMHI-SCI-ATBD-CMIC_v3_1_0 Page: 41/49
---	---	---

algorithm will still run if they are missing, but obviously with lower quality in snow-affected areas.

The NWP fields are obtained from operational ECMWF data or ERA-5.

4.5.2.8 *Sea ice concentration*

The concentration of sea ice is used for the cloud phase determination and to correct the albedo of sea for the presence of ice. It is obtained from the OSI-SAF (either operational products, or re-processed). The correction for sea ice is implemented in a similar way as for snow: $\alpha_s = \alpha_{s,ice} f_{ice} + \alpha_{s,water} (1 - f_{ice})$, where f_{ice} is the sea ice concentration and $\alpha_{s,ice}$ is the channel-dependent, prescribed sea-ice albedo. Like the snow parameters, the input of sea ice concentration input is not mandatory.

4.5.2.9 *Ozone*

A monthly mean total ozone column climatology at 1 x 1.5 degrees was generated from the Multi Sensor Reanalysis (MSR) dataset (Van der A et al., 2010). This is needed as input for the atmospheric correction. All ozone is assumed to reside above the clouds.

4.5.3. Description of Output

The output file contains nine datasets with products, five datasets with error estimates and three processing flags. Here, for each dataset in SAFNWC/PPS, the name, the data it contains and the units are listed. The physical data are implemented with scale factor, add offset and no-data-value, of which the values can be read in the file. All products except `cmic_phase` and `cmic_phase_extended` are available only in daylight conditions ($\theta_0 < 84^\circ$).

cmic_phase: Cloud-top thermodynamic phase, classes: liquid, ice

cmic_phase_extended: Cloud-top thermodynamic phase, extended to more classes.
Classes: clear, fog, water, super-cooled, mixed, opaque_ice, cirrus, overlap, overshooting (The class overshooting is TBD03)

cmic_lwp: Cloud liquid water path, unit: kg/m²

cmic_iwp: Cloud ice water path, unit: kg/m²

cmic_cwp: Cloud water path, unit: kg/m²

cmic_cot: Cloud optical thickness, dimensionless

cmic_cre: Cloud particle effective radius, unit: m (though typical values are in the μm -range)

cmic_cdnc: Cloud droplet number concentration, unit: m⁻³

cmic_cgt: Cloud geometrical thickness, unit: m

cmic_dewp: Error estimate for cloud water path, relates to `cmic_cwp`, but is also valid for `cmic_lwp` and `cmic_iwp`, unit: kg/m²

cmic_dcot: Error estimate for cloud optical thickness, relates to `cmic_cot`, dimensionless

cmic_dcre: Error estimate for cloud particle effective radius, relates to `cmic_cre`, unit: m

cmic_dcdnc: Error estimate for cloud droplet number concentration, relates to `cmic_cdnc`, unit: m⁻³

cmic_dcgt: Error estimate for cloud geometrical thickness, relates to `cmic_cgt`, unit: m

cmic_conditions: flag for geophysical and processing conditions, bit flag, described below

cmic_quality: flag for quality indicators, bit flag, described below

cmic_status_flag: flag for processing conditions and status, bit flag, described below

The formulations of the flags **cmic_conditions** and **cmic_quality** are common with the other SAFNWC/PPS PGEs, though the content is updated for CMIC (e.g., quality criteria are specific, while land/sea is the same for all PGEs). The formulation of the **cmic_status_flag** is specific for the CMIC product.

Table 17 CMIC conditions and processing flags

Bit number	Flag: cmic_quality	Explanation
0	Non-processed	Containing no data. Cloud-free pixel or pixel for which no product could be retrieved.
1	Spare	
2	Spare	
3-5	Quality	0: N/A nodata 1: Good 2: Questionable (Set when there is snow or ice at the surface or when the cloud phase has been changed by the optical properties retrieval) 3: Bad (Set when the NIR reflectance is outside the range of the look-up-table) 4: Interpolated/Reclassified (Set when the pixel has been reset to clear by the optical properties retrieval)
Bit number	Flag: cmic_status_flag	Explanation
0	Cloud-free	Cloud-free
1	Bad optical conditions	When the optical conditions are too bad for retrieving cwp, cot and cre (too high solar zenith angle)
2	Snow/ice	There is suspected snow or ice at the surface
3	1.6 micron used	The 1.6 μm channel has been used for the retrieval.
4	3.8 micron used	The 3.8 μm channel has been used for the retrieval.
5	2.1 micron used	The 2.1 μm channel has been used for the retrieval.
6	2.2 micron used	The 2.2 μm channel has been used for the retrieval.
Bit number	Flag: cmic_conditions	Explanation
0	Outside swath	Pixel is outside swath (can occur after remapping to region)
1-2	Illumination	day/night/twilight
3	Sunglint	possibly sun glint
4-5	Land Sea	land/sea/coast
6	High Terrain	high terrain

<i>EUMETSAT Satellite Application Facility to NoWCasting & Very Short Range Forecasting</i>	Algorithm Theoretical Basis Document for Cloud Micro Physics of the NWC/PPS	Code: NWC/CDOP3/PPS/SMHI/SCI/ATBD/CMIC Issue: 3.1.0 Date: 01 September 2022 File: NWC-CDOP3-PPS-SMHI-SCI-ATBD-CMIC_v3_1_0 Page: 43/49
---	---	---

7	Rough Terrain	rough terrain
8-9	Satellite input data	Satellite data is available/missing
10-11	NWP input data	NWP data (surface temperature and total water vapour) is available/missing
12-13	Product input data	Cloud mask data is available/missing
14-15	Auxiliary input data	Auxiliary data is available/missing

5. ASSUMPTIONS AND LIMITATIONS

In this section some of the assumptions and limitations associated with the retrieval algorithms are listed. There are also general limitations related to the characteristics of the satellite instruments. For example, GAC-AVHRR has a nominal resolution of $5 \times 4 \text{ km}^2$, compared to $1 \times 1 \text{ km}^2$ for LAC-AVHRR. A coarser resolution gives rise to systematic biases in the derived cloud physical properties, as outlined below. Also, polar orbiters have only two overpasses per day in the tropics (of which one during nighttime) and up to ≈ 8 near the poles. Thus, coverage of the diurnal cycle of cloud properties is limited.

Specific limitations for the cloud micro physics products include:

- The derivation of cloud optical properties from reflected solar radiation is dependent on the availability of daylight. This means that no retrievals of cloud optical thickness, cloud particle effective radius and liquid/ice water path can be done during night time. However, cloud phase can be (and is) retrieved during night time.
- Sun glint can affect the cloud property retrievals considerably, in particular for broken cloudy scenes over ocean. Therefore, possibly sun glint-affected pixels (defined by a scattering angle differing more than 25 degrees from the direct glint angle) over ocean are flagged.
- Cloud retrievals are performed assuming that clouds are plane parallel. This is true only in a minority of cases, which implies that retrieval errors become larger as clouds deviate from being plane parallel. Especially convective clouds can be problematic, as they frequently have illuminated and shadowed sides (see, e.g., Marshak et al. 2006). Broken and sub-pixel cloud fields, including cloud edges, can also cause problems for retrieving cloud properties, since a passive satellite sensor measures an averaged radiance of the cloudy and cloud-free part of a pixel. The error made in these cases is among others dependent on the contrast between clouds and underlying surface, the true properties of the cloud, and the cloud fraction within the sampling resolution of the instrument (Oreopoulos and Davies 1998; Coakley et al. 2005; Wolters et al. 2010).
- The retrieval is highly problematic over very bright surfaces, particularly ice and snow, as the visible reflectance from clouds is similar to that from the surface.
- Unlike active satellite instruments, which can derive cloud profile information, retrievals from passive satellite instruments are limited by the fact that the obtained signal emanates from the integrated profile. Since near-infrared radiation is only penetrating into the cloud to a certain depth (due to absorption by cloud particles), the retrieved cloud phase and cloud particle effective radius are representative for the upper part of the cloud (Platnick 2001). The penetration depth depends on the amount of absorption by cloud particles, which overall increases with wavelength. This means that the retrieved CPH and r_e depend on which NIR spectral channel is used (in our case 1.6, 2.2 or $3.8 \text{ }\mu\text{m}$). See, for example, Rosenfeld et al. (2004) for a discussion on pros and cons of the use of different NIR channels. Seethala and Horvath (2010) and Zhang and Platnick (2011) noted that the $3.8 \text{ }\mu\text{m}$ r_e can be significantly

<i>EUMETSAT Satellite Application Facility to NoWCASTing & Very Short Range Forecasting</i>	Algorithm Theoretical Basis Document for Cloud Micro Physics of the NWC/PPS	Code: NWC/CDOP3/PPS/SMHI/SCI/ATBD/CMIC Issue: 3.1.0 Date: 01 September 2022 File: NWC-CDOP3-PPS-SMHI-SCI-ATBD-CMIC_v3_1_0 Page: 44/49
---	---	---

smaller than the 1.6 or 2.2 μm r_e in non-raining stratocumulus (Sc) clouds, for which one would expect, in contrast, a steady increase in r_e from 1.6 through 2.2 to 3.8 micron. They suggested that drizzle and/or 3D inhomogeneity effects might be the cause. Zhang et al. (2012) further investigated the effects of drizzle and cloud horizontal inhomogeneity on MODIS r_e retrievals using Large Eddy Simulation (LES) models and synthetic retrievals and found that drizzle does not have a strong impact but inhomogeneity, the plane-parallel bias, does.

- In the derivation of equations (3) for LWP and eq. (7) for IWP it is assumed that the cloud particle effective radius is vertically uniform. On the other hand, the ISBLC model used to derive CDNC and CGT, yields an increasing effective radius with height. While Sc clouds normally obey (sub-)adiabatic theory, leading to vertical profiles as in the ISBLC model, this is typically not the case for cumulus clouds, which tend to have a more uniform vertical profile (see Grosvenor et al., 2018 and references therein). Deviations from vertical homogeneity are also common for ice clouds. Thick ice clouds often have small ice crystals at the top, which are not representative of the full vertical extent. As a consequence, IWP can be underestimated in these cases. Results are even more questionable for multi-layer cloud systems. Here the derived effective radius (uppermost cloud) may be totally unrelated to any cloud below, so the relation between r_e and LWP/IWP is not applicable here.
- Aerosols are not considered in the CMIC retrieval. This assumption is usually justified because aerosols reside below or within the cloud and their optical thickness is small compared to that of the cloud. However, if the aerosols reside above the cloud and if they are sufficiently absorbing, they can significantly lower the visible reflectance. The effect on the retrievals depends on the channel combination used and on the aerosol properties (Haywood et al. 2004). The impact is strongest for the 1.6- μm channel, with a possible underestimation of r_e by several microns. For the 3.8- μm channel, the impact is smaller and can be an overestimation of r_e . Cloud optical thickness generally has a low bias. Although the annual mean effect of absorbing aerosols is relatively small, their instantaneous effect on LWP can be as high as a 40 g m⁻² low bias, mostly caused by a reduction in optical thickness. Wilcox et al. (2009) and Seethala and Horvath (2010) both have given estimates of absorbing aerosol effects on MODIS LWP by comparing it with passive microwave retrievals and quantifying the aerosol load with the help of OMI aerosol index.
- Precipitation may have an effect on cloud property retrievals in case the radiation penetrates sufficiently deep into the cloud to be affected by the (large) precipitating droplets. Retrievals with the 1.6- μm channel are expected to be most sensitive to this, but synthetic studies (e.g., Zinner et al. 2010; Zhang et al. 2012) have not indicated significant impact on the effective radius retrieval.
- Many assumptions are made for the calculation of LUTs with DAK. These include: the absence of aerosols, the location of liquid clouds between 1 and 2 km height and of ice clouds between 5 and 6 km height, the specific habits and resulting phase functions of ice crystals, and the type and width of water droplet effective radius distributions. The necessity of these assumptions is an illustration of the heavily underconstrained nature of the cloud micro physics retrieval principle.
- While the cloud phase product has been validated for instantaneous values against Calipso data over both land and sea, the LWP product has only been properly validated for instantaneous values over sea using AMSR-E data. However, comparisons with MODIS liquid water path, split in land and sea, have also been made, showing about as good performance over land as over sea. See the Validation report for detailed validation results, and a discussion of validation over land [RD.4].

<i>EUMETSAT Satellite Application Facility to NoWcasting & Very Short Range Forecasting</i>	Algorithm Theoretical Basis Document for Cloud Micro Physics of the NWC/PPS	Code: NWC/CDOP3/PPS/SMHI/SCI/ATBD/CMIC Issue: 3.1.0 Date: 01 September 2022 File: NWC-CDOP3-PPS-SMHI-SCI-ATBD-CMIC_v3_1_0 Page: 45/49
---	---	---

- The usage of channel 2.2μm has not yet been validated (PPS vEPSSG-SAFbeta3).

<i>EUMETSAT Satellite Application Facility to NoWCASTing & Very Short Range Forecasting</i>	Algorithm Theoretical Basis Document for Cloud Micro Physics of the NWC/PPS	Code: NWC/CDOP3/PPS/SMHI/SCI/ATBD/CMIC Issue: 3.1.0 Date: 01 September 2022 File: NWC-CDOP3-PPS-SMHI-SCI-ATBD-CMIC_v3_1_0 Page: 46/49
---	---	---

ANNEX A. List of TBC, TBD, Open Points and Comments

TBD/TBC	Section	Resp.	Comment
TBD02	4.2.1, 4.3.1.2, etc.	KNMI	<p>The METimage processing is not included in PPS v2021 (a.k.a. the second beta-release of PPS vEPSSG). And for VIIRS only AVHRR-heritage channels are used in PPS v2021.</p> <p>For EPS-SG third beta version (to be released as a patch of PPS v2021): beta capability for METimage processing is planned to be included using heritage channels and optionally the 2.2µm channel for effective radius calculation.</p> <p>Closed in PPS vEPSSG-SAFbeta3, as well as for vEPSSG</p>
TBD03	4.2.1, 4.3.1.2, etc		More METimage channels will be considered for inclusion in PPS vEPSSG-day2.

ANNEX B. Thresholds used in the cloud phase algorithm

The cloud phase algorithm described in Section 4.3.1 contains a number of thresholds, the settings of which are detailed here.

NIR_PHASE_THRES

Channel	Water or snow/ice	Other
1.6 μm	0.17	0.32
3.8 μm	0.06	0.06

NIR_CIRRUS_THRES

Channel	Water or snow/ice	Desert	Other
1.6 μm	0.20	0.55	0.33
3.8 μm	0.12	0.40	0.12

NIR_OVER_THRES

Channel	Snow/ice	Other
1.6 μm	0.17	0.0
3.8 μm	0.06	0.0

BTD1112_DOVERLAP_THRES

- $0.35 \leq R_{0.6} \leq 0.60$: $\text{MAX}(a_0 + a_1 R_{0.6} + a_2 (R_{0.6})^2 + \dots + a_4 (R_{0.6})^4, \text{MIN_BTD1112_DOVERLAP}) - 0.1$
- $0.60 < R_{0.6} < 0.90$: $\text{MIN_BTD1112_DOVERLAP} - 0.1$

If $R_{0.6} < 0.35$ or $R_{0.6} \geq 0.90$, the threshold is not applied. In addition, for latitudes poleward of 65 degrees, and if $R_{3.8} > 0.2$, the threshold is not applied.

The coefficients a_0 to a_4 and MIN_BTD1112_DOVERLAP are functions of θ and θ_0 (in 10-degree bins)

a_0

$\theta \backslash \theta_0$	0-10	10-20	20-30	30-40	40-50	50-60	60-70
0-10	2.94	3.14	3.15	3.03	3.27	3.77	3.77
10-20	2.94	3.14	3.15	3.03	3.27	3.77	3.77
20-30	2.76	3.04	3.14	3.20	3.23	3.25	3.25
30-40	2.95	2.75	3.03	3.15	3.34	3.48	3.48
40-50	2.62	2.71	2.65	2.80	2.80	2.97	2.97
50-60	2.26	2.59	2.33	2.43	2.62	3.01	3.01
60-70	1.94	1.29	1.65	1.65	1.88	0.649	0.649
70-80	-2.33	-1.83	0.417	-2.67	-0.72	0.234	0.234

a_1

$\theta \backslash \theta_0$	0-10	10-20	20-30	30-40	40-50	50-60	60-70
0-10	.936	-3.25	-2.60	1.71	-.743	-8.27	-8.27
10-20	.936	-3.25	-2.60	1.71	-.743	-8.27	-8.27
20-30	4.48	-1.20	-2.31	1.98	.148	2.65	2.65
30-40	.365	4.94	-.240	1.20	-2.60	-2.09	-2.09
40-50	6.62	4.96	6.72	5.76	8.27	9.71	9.71
50-60	12.1	6.67	11.2	10.5	9.62	7.24	7.24
60-70	16.7	24.5	19.9	19.9	18.1	33.7	33.7
70-80	69.2	62.6	35.3	65.7	45.8	35.6	35.6

a_2

θ θ_0	0-10	10-20	20-30	30-40	40-50	50-60	60-70
0-10	-41.2	-24.1	-27.7	-45.7	-36.0	-8.56	-8.56
10-20	-41.2	-24.1	-27.7	-45.7	-36.0	-8.56	-8.56
20-30	-54.7	-32.0	-27.7	-29.6	-38.0	-52.9	-52.9
30-40	-37.6	-55.1	-34.1	-30.1	-24.0	30.2	30.2
40-50	-60.8	-53.0	-57.7	-53.8	-64.1	-76.7	-76.7
50-60	-81.4	-59.6	-72.9	-65.9	-62.1	-48.8	-48.8
60-70	-102	-127	-106	-100	-93.7	-138	-138
70-80	-309	-280	-169	-256	-186	-123	-123

θ θ_0	0-10	10-20	20-30	30-40	40-50	50-60	60-70
0-10	-50.9	-38.3	-42.0	-55.2	-48.0	-31.6	-31.6
10-20	-50.9	-38.3	-42.0	-55.2	-48.0	-31.6	-31.6
20-30	-60.2	-43.6	-40.1	-41.4	-46.7	-63.6	-63.6
30-40	-46.7	-58.1	-42.0	-37.9	-32.5	-41.1	-41.1
40-50	-62.5	-54.9	-54.2	-49.9	-56.3	-71.3	-71.3
50-60	-77.2	-60.2	-62.8	-51.3	-47.0	-32.2	-32.2
60-70	-100	-112	-89.6	-76.5	-70.4	-84.0	-84.0
70-80	-285	-252	-149	-182	-128	-52.1	-52.1

MIN_BT D1112_DOVERLAP

a_4

θ θ_0	0-10	10-20	20-30	30-40	40-50	50-60	60-70
0-10	85.8	60.5	66.9	93.5	79.1	42.4	42.4
10-20	85.8	60.5	66.9	93.5	79.1	42.4	42.4
20-30	105	71.5	65.0	67.8	79.2	107	107
30-40	78.8	103	71.6	64.7	54.6	68.2	68.2
40-50	111	97.9	101	93.7	108	133	133
50-60	141	108	120	103	96.3	70.1	70.1
60-70	178	208	170	153	143	187	187
70-80	508	455	275	369	266	140	140

θ θ_0	0-10	10-20	20-30	30-40	40-50	50-60	60-70
0-10	0.70	0.70	0.70	0.70	0.75	0.80	0.80
10-20	0.70	0.70	0.70	0.70	0.75	0.80	0.80
20-30	0.70	0.70	0.70	0.70	0.75	0.80	0.80
30-40	0.70	0.70	0.70	0.70	0.75	0.80	0.80
40-50	0.70	0.70	0.70	0.70	0.75	0.80	0.80
50-60	0.70	0.70	0.70	0.70	0.75	0.90	0.90
60-70	0.75	0.75	0.75	0.80	0.80	0.90	0.90
70-80	0.75	0.75	0.75	0.80	0.80	0.90	0.90

a_3

<i>EUMETSAT Satellite Application Facility to NoWCasting & Very Short Range Forecasting</i>	Algorithm Theoretical Basis Document for Cloud Micro Physics of the NWC/PPS	Code: NWC/CDOP3/PPS/SMHI/SCI/ATBD/CMIC Issue: 3.1.0 Date: 01 September 2022 File: NWC-CDOP3-PPS-SMHI-SCI-ATBD-CMIC_v3_1_0 Page: 49/49
---	---	---

$BTD1112_CIRRUS_THRES = \text{MAX}(1.0, \text{MIN}(b_0 + b_1 T_{11} + b_4 (T_{11})^2 + \dots + b_4 (T_{11})^4, 4.0),$

The coefficients b_0 to b_4 are the following functions of θ (in 10-degree bins):

θ coeff	0-10	10-20	20-30	30-40	40-50	50-60	60-70
b_0	-3.21578e3	-2.94035e3	-3.21256e3	-3.47061e3	-3.50486e3	-5.08847e3	-5.09507e3
b_1	4.88463e1	4.47332e1	4.86994e1	5.27678e1	5.32849e1	7.75359e1	7.80031e1
b_2	-2.76528e-1	-2.53526e-1	-2.75139e-1	-2.99072e-1	-3.01970e-1	-4.40956e-1	-4.45700e-1
b_3	6.90693e-4	6.33594e-4	6.85787e-4	7.48048e-4	7.55160e-4	1.10843e-3	1.12561e-3
b_4	-6.41179e-7	-5.88096e-7	-6.35206e-7	-6.95628e-7	-7.02035e-7	-1.03800e-6	-1.05900e-6

EMS38_PHASE_THRES

$T_{11} \leq 245$: 0.9

$T_{11} > 245$: 1.12

BTD1112_NOVERLAP_THRES_H/_L and EMS38_NOVERLAP_THRES_H/_L

	-30 < latitude < 30	latitude > 30
BTD1112_NOVERLAP_THRES_H	2.5	2.0
BTD1112_NOVERLAP_THRES_L	0.78	0.58
EMS38_NOVERLAP_THRES_H	5.0	2.0 (over water: 2.5)
EMS38_NOVERLAP_THRES_L	1.1	1.0 (over water: 1.05)

These thresholds are not applied if $T_{3.8} - T_{11} \leq 0$ or if the surface type is desert.